Promises and Challenges of Grid Forming: Transmission System Operator, Manufacturer and Academic View Points

Carmen Cardozo*, Thibault Prevost*, Shun-Hsien Huang†, Jingwei Lu‡, Nilesh Modi‡,
Masaya Hishida§, Xiaoming Li§, Adil Abdalrahman¶, Pär Samuelsson¶, Thierry Van Cutsem‖,
Yorgo Laba**, Yahya Lamrani**, Frederic Colas** and Xavier Guillaud**
* R&D, *Réseau de Transport de Electricité* (RTE), 92073 La Defense, France
† Electric Reliability Council of Texas (ERCOT), Austin, Texas, 76574, USA
‡ Australian Energy Market Operator (AEMO), Brisbane, Qld. 4000 Australia
§ Zenobē Energy, WC2N 6DU London, U.K.
¶ Hitachi Energy - HVDC, Lyviksvägen 3, 771 80, Ludvika, Sweden
‖ independent consultant, Liège, Belgium
** Univ. Lille, Arts et Metiers Institute of Technology, Centrale Lille, Junia ULR 2697 - L2EP 59000 Lille, France
Corresponding author: Xavier Guillaud (xavier.guillaud@centralelille.fr)

***Abstract*—With the increasing penetration of power electronic converters in the power system induced by the energy transition, Grid Forming (GFM) technology emerges as crucial for complementing traditional synchronous generators in fulfilling system needs. All over the world, TSOs have started introducing performance-based requirements to define the desired behaviour of GFM units without prescribing specific technical solutions. Based on these specifications, manufacturers design there grid-connected equipment. However, depending on requirements, challenges may arise in optimizing control strategies without hardware modifications, potentially becoming cost-driving factors. Intellectual property protection limits information disclosure, restricting the guidance available to TSOs during cost-benefit assessments. Academic contributions on GFM control and generic models can bridge the gap, providing a fair portrayal of the general behaviour and then facilitates an open discussion on their ability to meet the requirements and contribute to fulfil system needs. This survey paper provides a comprehensive overview of the perspectives offered by these diverse stakeholders.**

***Index Terms*—BESS, Grid forming, HVDC, system needs.**

I. Introduction

As we progress through the energy transition and the deregulation of the electricity sector, a growing imperative arises to align system needs with available resources capable of meeting them. Their timely deployment and optimal real-time utilization are crucial to ensure an affordable and reliable power supply over time. In this context, Grid Forming (GFM) can be seen as a technology with the potential to be deployed in various resources, including Power Park Modules (PPM), Battery Energy Storage Systems (BESS) and Flexible AC Transmission Systems (FACTS), to complement Synchronous Generators (SG) in fulfilling specific system needs [1]–[4].

Submitted to the 23rd Power Systems Computation Conference (PSCC 2024).

From the Original Equipment Manufacturer (OEM) perspective, requirements related to desired performance rather than requirements on the detailed control structure are preferred. Consequently, in recent years, various Transmission System Operators (TSOs) worldwide have introduced performance-based requirements to define the desired behaviour of GFM units without prescribing specific technical solutions, particularly on the control strategy and the associated resource [5]–[7]. This task involves projecting system-wide needs into requirements for individual assets. Key challenges encompass avoiding unnecessary constraints that could prevent OEM from delivering cost-effective solutions while ensuring that they ultimately comply with the proposed requirement set and that they can effectively address system-wide needs.

System developers and OEM design technical solutions based on detailed specifications and a profound understanding of equipment constraints. As requirements accumulate, challenges may arise in optimizing control strategies without resorting to hardware modifications, potentially becoming cost-driving factors for the installation design. The details of these technical solutions are often subjected to Intellectual Property (IP) protection, limiting the information these parties are prepared to disclose and, consequently, restricting the guidance available to TSOs during cost-benefit assessments.

To bridge the gap, academic contributions on GFM control and generic models could provide a fair portrayal of the general behaviour of the technical solutions depending on the actual representation. This facilitates an open discussion on their ability to meet the requirements and contribute to fulfil system needs, while shedding lights on the burden new requirements may impose on specific devices. While generic models offer valuable insights into the overall system behaviour, more precise vendor models are always required for detailed design studies.

This paper gives voice to representatives of these various stakeholders and presents their views in an articulated manner. It is organised as follows: Section II examines the motivations behind fostering GFM adoption. Subsequently, Section III discusses the subtleties of GFM technical specifications in different regions to meet local needs. Afterwards, Section IV gives an overview of GFM deployment on BESS, while Section V brings forward the challenges of implementing this solution on High Voltage Direct Current (HVDC) transmission systems. Following that, Section VI provides an academic perspective on defining generic models and testing them in various situations. Finally, conclusion are drawn in Section VII.

II. From the TSOs' lens: quantifying and fulfilling system needs

The responsibilities of different TSOs may vary slightly from one country to another, depending, for instance, on whether they own the grid infrastructure or not. Nevertheless, these responsibilities generally include ensuring cost-effective security of power supply — an endeavor easier said than done, requiring coordinated actions across a wide range of time frames. Hence, before delving into the latest advancement on GFM as a technical solution and the constraints it poses on product developers, this section revisits the prerequisites essential for the *proper* functioning of power systems.

For this purpose, Section II-A first recalls the comprehensive nature of system needs and elaborates on Key Performance Indicators (KPI) allowing their quantification. Subsequently, Section II-B presents ongoing developments toward the consideration of these KPI in the decision-making process. Finally, Section II-C outlines the resources that can actively contribute to the satisfaction of the identified system needs. In particular, we focus on the aspects in which GFM technologies will play a pivotal role. Challenges related to the transition to *variable* energy sources and the increasing need for flexibility resources to maintain power balance across different time scales are topics beyond the scope of this work, although they are acknowledged to be significant concerns for TSOs.

A. Defining and quantifying system needs

In this section, we discuss the system needs related to power system security. Beyond power balance, load sharing, and classical ancillary services such as frequency and voltage regulation, these needs include:

1) AC voltage (maintain fundamental frequency),
2) inertia (providing time for regulation and defense actions based on system observation),
3) fast fault current (for protection and voltage support during short-circuits),
4) system strength (in the sense of low $\frac{dV}{dI}$),
5) robustness (to different grid conditions),
6) stability:
   - transient stability,
   - small-signal stability (positive damping),
7) withstand capabilities (according to risk policies), and
8) restoration capabilities.

Similar lists have been proposed in [1], [3]. Here, we present an overview of the diverse factors involved in their quantification from the perspective of three TSOs, operating systems of various characteristics, namely the Australian Energy Market Operator (AEMO), the Electric Reliability Council of Texas (ERCOT) and *Réseau de Transport d'Electricité (RTE)*.

1) AC fundamental frequency voltage: TSOs deliver AC voltage to customers. The frequency and depth of perturbations such as low/high voltage events, as well as the harmonic content, serve as quality KPI. Contractually binding thresholds may apply to prevent malfunctions or tripping of grid users. Some of these events could jeopardize system security if they lead to large power imbalances. These indicators are often monitored with specific devices at sensitive location [8].

2) Inertia: refers to the power system's ability to resist changes in frequency following power imbalances. It is often quantified as an energy buffer, usually measured in MWs. Another classical indicator used in this context is the Rate of Change of the Frequency (RoCoF), expressed in Hz/s. Limiting its maximal value, hence maintaining a minimal level of inertia, is important for various reasons:

- To allow sufficient time for primary frequency control to restore power balance. This need may be reduced by the development of Fast Frequency Response (FFR) services.
- To avoid disconnection of RoCoF sensitive units.
- To ensure that the frequency can be accurately measured by any device on the grid that relies on this signal.
- In particular, to provide time for the execution of defense plans, namely Under Frequency Load Shedding (UFLS) schemes, in the event of disturbances exceeding the system's Frequency Containment Reserve (FCR).

The state-wide blackout experienced by South Australia (SA) on September 28, 2016, is a well-known example of the risk associated with an inertia shortfall. Approximately 850,000 SA customers lost electricity supply, including households, businesses, transport, community services, and major industries. This event occurred after the SA power system was separated from the rest of the Australian National Electricity Market (NEM) power systems, which was triggered by multiple factors, including severe weather conditions [9]. After the SA separation, there was a deficiency in the electricity supply within the SA island, which caused a rapid frequency reduction with a RoCoF at 6 Hz/s, beyond the capability of the local UFLS scheme for arresting the frequency in-time, and an eventual system-wide blackout. Based on extensive power system simulations conducted by AEMO during subsequent event investigations, it was suggested that keeping the RoCoF below 3 Hz/s could have reliably preserved the frequency in the SA island [10]. However, achieving a lower RoCoF was not possible due to the very low level of inertia available in the SA island on September 28, 2016. Following these findings, recommendations by AEMO were implemented in collaboration with the local Network Service Providers (NSP) in SA, including the design of Special Protection Schemes (SPS) to manage the risk of SA separation, and a RoCoF-based UFLS system.

3) Fast Fault Current: historically, Synchronous Machines (SM) have provided high and fast current in response to grid event. The system has been designed to handle such high current and has also taken benefit of it to design simple protection schemes. This property facilitates selectivity, allowing for quick fault detection and clearance while disconnecting the minimum amount of devices. Additionally, it helps limiting voltage drop along the network, thereby improving quality for customers by reducing flicker and limiting the spread of short undervoltage events. Understanding the injected current by Power-Electronic Interfaced Resources (PEIR) is essential for deducing fault information from the current waveform. In general, PEIR are required to inject fault current up to their rated capacity [11], with specific details about the expected dynamic behaviour outlined in different standards, such as the IEEE Std 2800-2022 [12] and the EN 50549-2 [13]. Due to the limited current capability of PEIR, priority rules have traditionally favoured reactive current during faults to support voltage. However, with their growing share, concerns about potential frequency-related events resulting from substantial reductions in active current are prompting a reassessment of this practice in certain regions [14]. Moreover, the notion of system strength, detailed below, has been traditionally correlated with the fault current due to the inherent properties of SM. In the Australian NEM for instance, the minimum three phase fault currents are used as a proxy for system strength at the fault level nodes which are selected as per the system strength requirements methodology [15]. In a broader context, as PEIR respond distinctly to system events, particularly for small and large disturbances, it becomes imperative to differentiate fault behaviour from system strength.

4) System strength: more generally AEMO defines system strength as *the ability of the power system to maintain and control the voltage waveform at any given location in the power system, both during steady state operation and following a disturbance* [16]. Although conventionally associated with the concept of Short-Circuit Power (SCP) in SM-dominated power systems, it is more related to voltage stiffness, represented by the voltage excursions resulting from injected current variations. For this reason, it is often assimilated to an impedance. We refer to strong and weak grid conditions for scenarios with high and low SCP, translating to low and high grid connection impedance, respectively. This characteristic naturally affects power quality, but also small signal stability (SSS).

- The association of power quality with system strength is occasionally emphasized by traditional customers using induction machines, which can cause significant voltage drops during the startup process, potentially leading to equipment malfunctions of other users in weak grids.
- While the relationship between system strength and SSS has gained attention with the massive connection of PEIR [17], the SSS of remote generation based on large SM has also been a subject of historical scrutiny. These concerns nonetheless faded as power systems became increasingly interconnected, and the widespread adoption of Power System Stabilizers (PSS) took precedence.

As for quantifying the system strength, another indicator is typically used: the Short-Circuit Ratio (SCR). It normalizes the *available* SCP at a specific location with respect to the nominal power of a certain facility. Different variants of this indicator have been defined to account for PEIR, including the Effective SCR (ESCR), the Weighted SCR (WSCR), the Generalized SCR (gSCR) among others [18]–[23]. Similar to the arguments presented for the AC voltage need, we could say that TSOs have been expected to *provide* a certain level of SCP to their customers. Technical specifications and connection agreements typically precise minimal and maximal values, thereby defining the range for which the installation is designed to operate correctly. However, similar to inertia, this *service* has been taken for granted in SM-dominated systems, and the means for TSOs to marginally adjust it are often limited to topological changes. Additionally, defining scenarios for calculating available SCP and compiling relevant data representative of the system's evolution over decades has always been challenging [24].

a) AEMO experience: in Australia, there have been a few PEIR driven sub-synchronous oscillation incidents due to the lack of system strength at the vicinity of these PEIR. One notable incident involved five nearby solar farms, ranging from 50MW to 90MW, connected to 66 kV distribution systems in a remote area of the Australian NEM power system. The loss of a nearby 220kV transmission circuit resulted in a low system strength condition for this area, and caused the five solar farms to contribute to a 7 – 8 Hz sub-synchronous voltage oscillation with a magnitude of 0.8% to 1.0% of the nominal value, observable at the 220kV transmission substations in this area [25]. The oscillation was eliminated after upgrading the inverter control systems of the five solar farms with a solution developed in collaboration between AEMO and the OEM.

b) ERCOT experience: similarly, the integration of PEIR has led to the reduction of system strength, resulting in undesired oscillatory responses and unexpected unit trips in recent years. The Odessa I and II events, occurred in 2021 and 2022, are examples of this phenomenon [26], [27]. In addition, various localized oscillations among PEIR or interactions with grid elements have also been observed.

c) RTE experience: in France, historically, large generators (starting from 800 MW) are required to operate with a grid-connection impedance of up to 0.6 pu. [28], equivalent to a SCR of 1.67. This requirement emerged due to the development of larger Nuclear Power Plants (NPP) in remote locations with radial networks. Conversely, for smaller units (below 50 MW), a minimum SCR of 5 (corresponding to $X_{sc}^{max} = 0.2$ pu.) has been defined. Current efforts are focused on evaluating the necessity of revisiting these requirements.

5) Robustness: the electrical system undergoes continuous changes. Residual load follows consumption and distributed generation patterns and dispatchable generation is constantly being adjusted based on market and regulation processes. Simultaneously, operators modify the grid topology to manage security constraints. These factors contribute to an ever-increasing volatility in line flows and voltage profiles, in

Europe accentuated by the expanding cross-border exchange capacity. Moreover, preventive actions may be replaced by corrective measures to reduce operational costs, placing increased demand on the regulating and protective layers [29]. Consequently, the system may experience more frequent temporary excursions into exceptional operating conditions. Although timely handled by suitable remedial actions, RTE has, for instance, witnessed an increase in the overall number of one-off cases of 225 and 400 kV overload, particularly at the French-Spain border and for the N-1 scenario [30]. The increasing voltage and frequency volatility, especially in the transient time frame during and right after the disturbance, could trigger the protection and/or cause the PEIR to temporarily reduce the support or disconnect from the grid. Therefore, now, more than ever, all grid-connected devices must demonstrate desired performance across a wider range of operating conditions. ERCOT has, for instance, proposed more robust technical requirements, essentially to align with IEEE 2800-2022.

6) Stability: TSOs ensure large-scale power system stability by implementing actions across various time frames, from planning to real-time operation. In the short-term, the acceptability of system-wide operating points, in accordance with a given risk policy, is often determined through contingency analyses supported by time-domain simulations. Therefore, TSOs rely on accurate models and suitable simulation tools to assess the dynamic behaviour of the power system. Predefined mitigation measures, including topology or eventually more costly dispatch changes, are implemented when needed based on the monitoring of specific KPI. However, the integration of distributed PEIR complicates the task of maintaining a relevant system representation and identifying effective remedial actions. Moreover, the growing variability and uncertainty in operating conditions make traditional offline stability assessments increasingly inadequate. Therefore, the incorporation of more conservative assumptions becomes necessary to accommodate diverse system conditions, generating in turn a potential risk of infeasible situations. To cope with these challenges, various TSOs, are in the process of deploying online Dynamic Security Assessment (DSA) tools [29]. On the Australian side, in accordance with the National Electricity Rules (NER), AEMO is responsible for managing power system security on the eastern coast of the NEM power system following the AEMO's Power System Security and Power System Stability Guidelines [31], [32]. Practical implementation involves integrating linear constraints into the market dispatch engine. They represent static and dynamic limitations, covering voltage collapse as well as transient and oscillatory stability considerations. These constraints are derived from limit advice provided by regional NSP and their effective enforcement is verified through simulation. Updates occur as needed, typically when connecting a new generator.

Finally, during the planning stage, assessing instability risk proves exceptionally challenging due to the unavailability of accurate dynamic models for future assets, and uncertainty surrounds their specific locations in the grid. In practice, TSOs uphold system stability in the long term through performance-based grid connection requirements. In between, adjustments of protection settings may provide operators with additional flexibility to adapt to changing conditions [33].

a) Transient stability: technical requirements commonly applied to generation units focus on ensuring stability during faults of specified types, depth, durations, clearance and topology under the most challenging operating conditions. The fault duration to be considered for a particular installation is dictated by the system overall protection scheme, and must be included in the withstand capabilities. In France, for instance, units connected to the high voltage grid are required to withstand faults lasting 150 ms, while the requirement is reduced to 85 ms for the extra high network (above 110 kV), and it might be extended up to 250 ms in other EU countries [11]. In anticipation, the impact of PEIR on the transient stability of the remaining SG is assessed. In this context, accelerating real-time evaluations of Critical Clearing Time (CCT) to cope with the growing number of possible states is an active area of research [34], along with the optimisation of corrective actions.

b) Small-signal stability (positive damping): RTE has traditionally applied stability margin requirements based on frequency domain studies to ensure the proper damping of SG natural (local) modes [28], which have often defined PSS design. In Continental Europe (CE), concerns about interarea oscillation phenomena have led to the requirement of Power Oscillation Damping (POD) functions to PEIR in the latest Connection Network Codes (CNC) update [6]. For HVDC systems, inherent damping and Sub Synchronous Damping Control (SSDC) requirements were introduced in 2016 in addition to POD specifications [35]. Damping thresholds are enforced by some TSOs, such as ERCOT, which sets a 3% damping requirement to all resources. If non-compliance is identified in studies, adjustments to PEIR control are required, often in collaboration with vendors. In real-time, if oscillations occur, PEIR may be directed to curtail or disconnect until the issue is resolved. With faster dynamics and the high proliferation of PEIR across the grid, the SSS phenomenon now also extends to higher frequency events and might require complementary methods for study and monitoring [36], [37].

c) Modelling requirements for stability studies: significant efforts have been undertaken by TSOs worldwide to enhance requirements for Root-Mean Square (RMS) and Electromagnetic Transient (EMT) time-domain models. There is a particular focus on their validation processes to ensure accuracy and robustness under various system strength conditions. In France, for instance, new requirements for RMS model validation align with the IEC 60400-27 standard [38], while scenarios are consistently defined with respect to EMT validation cases [39], [40]. On the Australian side, AEMO updated in 2018 its Power System Model Guidelines [41], introducing, for the first time, relevant requirements for EMT models of generators seeking connection in the NEM power systems. These guidelines were further updated in 2023 to include inverter-based loads [42]. Moreover, ERCOT perform periodic EMT studies for the regions with high penetration of PEIR in a weak grid condition to ensure the RMS tool adequacy [43],

[44]. Finally, obtaining PEIR linearised models suitable for SSS studies remains an open question [45], [46]

Other power system stability phenomena, such as voltage collapse, are excluded from the discussion since their evolution is not expected to be significantly influenced by the adoption of GFM solutions. The changes in these relatively slower events are more likely to be dictated by the shift in generation location, power flow patterns, and the modification of the dynamic behaviour of the load, along with the deployment of sufficient regulation capabilities.

7) Withstand capabilities: in addition to the stability requirements defined for specific events and discussed in paragraph II-A6a, grid-connected devices and their associated auxiliary equipment must ride through a broader range of disturbances. They extend beyond short-circuits, to cover for potentially more constraining scenarios like evolving faults, generator disconnections, and changes in grid topology. These events lead to fast transients in electrical quantities such as voltage dips/swells, frequency excursions, and phase shifts. Up-to-date requirements in European CNC include at least minimal RoCoF and Fault Ride Through (FRT) time-dependent profiles. Withstand capability involves stable functioning and prompt recovery to the previous operational point, but it does not necessarily fully specify performance criteria. Nonetheless, upper bounds on the active power recovery time of generating units have been enforced to prevent subsequent events, notably a frequency incident. Presently set to 2 seconds for PPM in France, it should soon be reduced to 1 second [6]. For HVDC systems, the required rise time (up to 90% of the pre-fault active power) is usually below 500 ms, set to 200 ms in France to limit transient stability constraints in nearby SG. Analogously, ERCOT initially established FRT capability in 2013. The requirement has evolved over the years to accommodate the growth and advancement of PEIR. Following IEEE 2800-2022, ERCOT has proposed revised FRT requirements for existing and new PEIR to ensure their ability to remain connected and provide necessary reliability support, including active and reactive support, during events.

8) Restoration capabilities: system restoration has historically relied on SG. For this purpose, islanding capability is usually mandatory for large SG connected to the transmission network [47], [48], and is regularly tested [30]. To some extent, this requirement has been extended to a specific category of PEIR, with the subtlety that at least a GFM source (a virtual SM), external to the installation, is supposed to be part of the island [11], [28]. For HVDC systems, black start capability is often required and tested during commissioning [49]. Although the participation of PEIR in system restoration is beyond the scope of this work, it is recognized as a relevant research topic for ensuring the resilient operation of future power systems.

In conclusion, the task of safeguarding power system security extends beyond the act of balancing power. In this context, system needs find definition in the complex equilibrium between the diverse immunity of grid-connected devices and the overall system performance. This performance includes, but is not limited to, the maximal RoCoF following power imbalances (tied to inertia) and the propagation of voltage disturbances (linked to the system strength). Concurrently, these characteristics depend on the properties of the very same grid-connected devices. Complicating this scenario is the recognition that *system* needs are inherently local and highly sensitive to various factors, such as the relative size of installations and system operating conditions — encompassing grid topology, instantaneous load, generation mix, and, in particular, their geographical location. Consequently, these needs, along with the availability of resources to fulfill them, practically become almost as volatile as the system itself.

Moreover, the limitations of physical components and the complex dynamics of the closed-loop system make it difficult to accurately quantify and, even more so, predict system needs. CNC addresses this challenge from two perspectives. On one hand, they aim to improve immunity of various technologies to alleviate constraints on system performance. On the other hand, they establish a baseline of responses required at the installation level to contribute to this overall system performance. Exhaustively defining these requirements necessitates a thorough understanding of the security management process, which is precisely the focus of the upcoming section.

B. Sizing and monitoring system needs

Over time, TSOs have diligently worked on defining suitable security thresholds for emerging system needs. This, in principle, would enable the *optimal* deployment and utilization of the resource pool. Building upon the overview previously presented, in this section, we initiate a critical examination of the practical implications of optimizing fundamental resources for the existence of the power system. We aim to underscore the complexity of extending DSA concepts to new phenomena associated to the integration of PEIR. For this purpose, we take a detour from the service-oriented framework, adopting a power system security management perspective.

1) On the security management of power systems: it relies preventive and corrective actions to meet specific reliability criteria. Consequently, it depends on our proficiency in:

- For preventive actions, precisely *forecasting* the system state within the time horizon determined by the delay in deploying preventive measures.
- For corrective actions, accurately *observing* the system state and having levers that can be fully deployed before protective actions are triggered.
- In both cases, making informed decisions regarding the *necessity*, *effectiveness*, and optimality of these actions.

These tasks become particularly challenging in systems facing increasing variability and uncertainty stemming from both the energy transition and the deregulation of the electricity sector [29]. Here, we focus only on the *decision-making* part, which embeds different dimensions. In particular, we are interested in three of them, which will be illustrated with the congestion management example:

- Choosing the KPI under scrutiny (e.g. line current).
- Defining the security threshold(s), which determine the need for action (e.g. maximum allowable values).

- Establishing the reliability criteria (or risk policy) that guides the aforementioned decisions (e.g. the N-1 rule).

The primary goal is to ensure that the KPI consistently remains below the security threshold in the event of any single line outage. This task unfolds in at least three key stages:

- In planning: system infrastructure design, often founded on prospective scenarios and simplified models.
- In anticipation: determination of preventive actions, relying on system state forecast and contingency analysis.
- In real-time: deployment of corrective actions when an unforeseen event occurs, based on the system observation.

One could assert that during the planning stage, the feasibility space is expanded, allowing for optimization as we approach real-time. In practice, this is the result of a trade-off between investments and operational costs. It is nonetheless worth highlighting that if the phenomenon of interest is neither predictable nor observable, or if available remedial actions cannot be timely deployed (controllable), the concept of its security *management* in operation loses its meaning. In this scenario, the fallback solution remains the incorporation of appropriate margins during the design phase. This aims to prevent the security criteria associated with the relevant KPI from becoming the binding constraint in real-time operation.

2) Assessing new security risks: specifically those emerging from the transition from SG to PEIR. This brings us back to the system needs listed in section II-A. Here, we extend our discussion beyond their quantification to their planning, prediction, and observation.

a) Reliability criteria: similar to how spinning reserves address the potential outage of generation and/or load to ensure power system security, this principle should be extended to all resources needed to maintain minimal system-wide performance at all times. Moreover, in addition to covering for the loss of predefined assets, other factors such as structural modifications in the grid topology, changes in the generation mix, or even the loss of the last synchronous link between two areas may prove crucial depending on the specific phenomenon under consideration. Furthermore, identifying pertinent Worst Case Scenarios (WCS) involves not only defining critical contingencies but also plausible states.

b) Time frame: system needs must be met by resources across every time horizon. For instance, to ensure power balance close to real-time, operational considerations include maintaining margins for various anticipation periods, depending on the activation time of associated flexibility levers [50]. Looking years ahead, this goal translates into ensuring that enough generation capacity is built; a task accomplished through load forecasting and adequacy studies. Scenario and risk-based approaches allow us to cope with uncertainty.

c) General considerations on screening indicators: assessing stability in systems with high share of PEIR necessitates substantial data and computing power. When these resources are limited, high-fidelity time-domain simulations may be replaced by simplified ones, to obtain (supposedly conservative) *screening indicators*, also referred to as proxies. They have proven useful both in the planning phase with a broad range of scenarios and in real-time operation to quickly deploy remedial actions if required. In the following paragraphs, we discuss the use of different inertia and system strength KPI in the TSOs' decision-making process.

3) Inertia screening indicators: the risk of inertia shortfall is under investigation on a years-ahead basis in several systems in Europe, US and Australia. Furthermore, the implementation of real-time monitoring has been explored in select systems, including the Nordic region [51] and the UK [52].

a) AEMO experience: on 19 September 2017, the Australian Energy Market Committee (AEMC) published a new rule [53] which requires AEMO to develop the inertia requirements methodology [54], and calculate the minimum level of inertia and the secure level of inertia for each inertia sub-networks based on the methodology, on an annual basis. An inertia shortfall forecast for at least a five-year window must be included, with the latest 2023 inertia report published in December 2023 [55]. Once a shortfall is declared by AEMO, the inertia service providers are responsible for providing the requirement levels of inertia services to fill the shortfall.

b) ERCOT experience: along with the integration of PEIR, the system inertia, focusing on the Synchronous Inertia (SI) provided by the online SM, has been closely monitored. In addition, critical inertia level needs to be maintained to manage the risk of UFLS activation under potential credible generation outages and prevent potential blackout. Considering that ERCOT peak load is 85 GW and the loss of 2800 MW must not trigger UFLS (first stage at 59.3 Hz), a threshold of 100 GW-s of SI has been identified through detailed system dynamic analysis. In order to maintain sufficient system SI, real-time and near term future inertia levels are displayed and operator procedures to commit the additional resources as needed have been implemented.

c) European Network of Transmission System Operators for Electricity (ENTSO-E) experience: CE has experienced a few system splits in the last decade resulting in load shedding [56], [57]. A dedicated working group conducted a study on the CE system [58], characterizing the RoCoF of different areas in the case of various system split scenarios within Europe. The combined effects of reduced inertia, associated to the increasing number of installed PEIR, and increased power exchanges lead to RoCoF values exceeding 1 Hz/s in both resulting areas for many scenarios and reaching up to 4 Hz/s. This situation poses a risk of defense mechanism misbehaviour, potentially leading to a Europe-wide blackout. Even lower RoCoF values may cause localized load shedding misoperation with reduced impact. The new version of the European CNC will ensure that PEIR will be able to ride through such events [6]. The potential need for specific operational procedures may be explored in the years to come.

4) System strength screening indicators: in spite of the challenges associated with the modelling of PEIR in SCP calculation tools [59], different indicators have been employed worldwide for both planning [21], [60] and operational studies.

a) AEMO experience: there are currently two categories of regulations that are used to ensure sufficient system strength is maintained in the NEM:

- System strength requirements: AEMO calculates minimum three phase fault currents at representative locations, called the fault level nodes, across the NEM using the System Strength Requirements Methodology [15]. They are reviewed and updated annually, and published in AEMO's annual system strength report (latest report at [61]), along with projected system strength shortfalls. Fault level shortfalls are addressed by Transmission NSP.
- System strength impact assessment: generators seeking connection to the NEM power systems must undergo the assessment as per the System Strength Impact Assessment Guidelines [62], to ensure they do not jeopardize the stable operation of the NEM under low system strength conditions. Otherwise, they must provide necessary mitigation measures as determined by the assessment.

In both cases, positive sequence fault current calculations are used to determine the required fault levels, and detailed assessment are conducted with large scale EMT simulations.

b) ERCOT experience: while a minimum system strength criterion has not yet been established, various processes and requirements are in place to secure the reliable connection and operation of PEIR. For instance, ERCOT employs the WSCR in real-time to manage wind generation in the Panhandle area, imposing limits on the maximum output that wind generation can export to ensure stable operation.

c) RTE experience: ESCR from [18] has been evaluated for 2030 French high PEIR scenario as illustrated in Fig. 1. Red and orange dots are nodes considered *at risk*, indicating areas where more detailed studies might be necessary. A concentration of very low ESCR is observed at the 90/63 kV level, primarily due to the consideration of renewable connection at lower voltages.

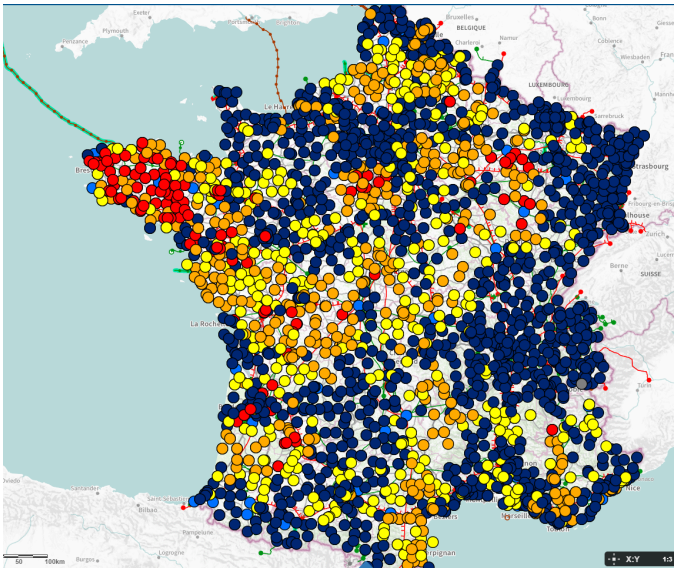

Fig. 1: Example of ESCR results on a French 2030 scenario

In conclusion, the evolution of system-wide security indicators has necessitated the establishment of minimal requirements — security limits — to ensure ongoing compliance with desired reliability criteria. To address system complexity and data unavailability, screening indicators have been adopted to distinguish acceptable situations from those requiring remedial actions, both in the planning and operational time horizons. Presently, these indicators primarily include inertia, as well as system strength and/or fault current.

SCR-based KPI show promise for long-term cost-benefit analyses and real-time system strength monitoring. However, there is no a singular and universally accepted definition of system strength and establishing security thresholds for selected indicators in PEIR-dominated grids requires careful consideration of the varying system conditions. On one hand, concerns persist about the conservatism of these KPI, which could lead to unnecessary costs as *weak* grid situations may not always pose stability risks. On the other hand, limited anticipation may result in resource scarcity and potentially expensive mitigation measures. Therefore, refining modelling hypotheses and gaining confidence in the validity of screening indicators are crucial for planning and real-time decision-making processes. Detailed time-domain simulations will always remain necessary at least for assessing remedial actions and conducting project-specific grid connection studies.

Despite advancements in the DSA field, security management strategies and tools may still be distant from accounting for dynamic phenomena beyond classical stability (frequency, voltage and transient stability), especially for considerably large interconnected systems. Regarding the service provision mechanism, thoughtful consideration of the nature of security constraints is necessary before drawing too much inspiration from existing solutions for the balancing problem. Finally, the *deployment* of the resource pool capable of fulfilling system needs must be carefully and robustly planned years in advance to ensure that enough capacity is always available. In the following, we examine how specific resources can (or cannot) provide services in line with the outlined system needs.

C. Fulfilling system needs

Most of the services previously discussed, including AC fundamental frequency voltage, system strength, inertia, and high and fast fault current, have been historically and inherently provided by SG as a by-product of electricity generation.

1) Limitations of conventional Grid Following (Gfl) PEIR: as PEIR displace the conventional SG fleet, the availability of these resource decreases, posing challenges for TSOs to maintain system stability under certain scenarios.

a) Inertia: it is recalled that, the *virtual* inertia, typically provided by Gfl converters, can be categorized as a fast frequency control. After a sudden event, the change of active power needs to be immediately handled by some unit with *true* inertia (grey area in Fig. 2 from [63]).

b) System strength: analogously, Gfl converters might be capable of providing fast voltage support but still rely on system observation. Transiently, their so-called *current*

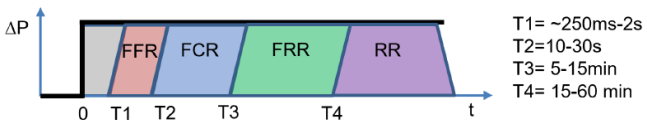

Fig. 2: Time frame difference for FFR and inertia

source behaviour or, more precisely, the potential interactions between the current loop and the Phase Locked loop (PLL) prevent them from contributing to the system strength and to the stability of nearby sensitive devices.

c) Fast Fault Current Injection (FFCI): when provided by Gfl converters, this function relies on voltage drop measurement to achieve a desired response $I_Q = f(V)$, which introduces a delay in the reaction including measurement time and control dynamics. Moreover, the injected current does not adapt to the grid impedance seen from the device. As a consequence, the impact of PEIR on the Short-Circuit Current (SCC) shape is notable. While SM exhibit an exponential decay in current, Gfl converters with I_Q control showcase a fast ramp followed by steady current. To the best of the authors' knowledge, there is no current record of protection mis-operation resulting from the reduced fault current infeed associated with the integration of PEIR. This absence of issues is likely attributed to the implementation of appropriate precautionary measures, indicating that current procedures and available technical solutions have proven reasonably effective so far. However, it's important to note that the concern persists [64]–[66] and that traditional indicators like I_k'' and I_b may no longer be relevant, as illustrated in Fig. 3.

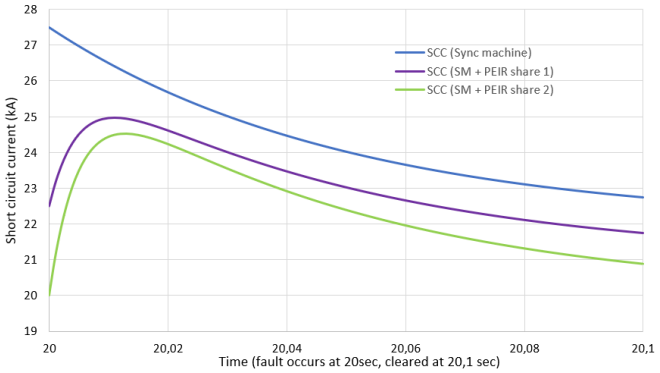

Fig. 3: SCC characteristics: Typical SM (blue), SM + Moderate Gfl (purple), SM + High Gfl (green)

d) Stability, robustness and withstand capability: maintaining a stable system at all times requires controls that are robust across a wide range of system conditions, which include coping with various system strengths. While Gfl converters, equipped with a PLL-based synchronisation mechanisms, can operate effectively in various system strength conditions with proper tuning, they may be prone to instability under specific tuning and varying system strength conditions.

2) Introducing GFM resources in the grid : under these circumstances, other grid users, such as PPM and certain loads, or service providers, through tenders [67], may contribute to providing these critical services. When they do, they will be referred to as *GFM resources*. Recent global development indicates that the GFM Inverters (GFMI) have emerged as a key technology which could assist TSOs in tackling challenges in the energy transition, including the reduction of SI and system strength. Additionally, TSOs can resort to the installation of dedicated devices to meet stability needs, namely Synchronous Condensers (SC) and specific FACTS with GFM capability, including HVDC systems. In this sense, ERCOT perform periodic EMT studies for the regions with high penetration of PEIR in a weak grid condition to assess the need for grid enhancement such as new circuit or SC, to mitigate the undesired and unexpected instability and generation outages.

In Great Britain (GB), National Grid (NG) Electricity System Operator (ESO) initiated in 2019 a competitive tender to procure long-term stability services from the service providers, spanning from the stability pathfinder phase 1 (SP1) to phase 3 (SP3). Through this process, NG ESO has secured:

- 12.5 GVAs of inertia in SP1 for 5-year contracts,
- 11.55 GVA of Short-Circuit Level (SCL) and 6.75 GVAs of inertia in SP2 for 10-year contract in Scotland, and
- 8.7 GVA of SCL and 17.08 GVAs of inertia in SP3 for 10-year contract in the England region.

GFMI-based technologies were invited to bid for the first time in the SP2 and two developers have secured the contract using GFM BESS solutions. The SCL is measured at 100 ms of FFCI after the transmission fault and assessed based on the multiple fault impedance and effectiveness between the Point of Common Coupling (PCC) and target nodes in the network. The *inertia*, in MVAs, is defined by multiplying the Inertia constant H as per Eq. (1) and the solution rating S_r.

$$H = \frac{\Delta P f_0}{2 S_r RoCoF} \tag{1}$$

where ΔP is the designed active power change during a frequency event and f_0 is the pre-fault system frequency. In order to measure the inertia, *Active RoCoF Response Power* is used for a RoCoF of less than 1 Hz/s, assessed under multiple operational conditions prior to a disturbance.

a) AEMO experience: NSP may choose to procure or contract SC as means to ensure the required fault levels. In addition, generators identified with adverse system strength impact may choose to remediate by installing SC. Moreover, a Voluntary Specification for GFMI [7], has been developed by AEMO in collaboration with industry partners and market participants, where the provision of inertia is expected to be a *core* capability. Furthermore, AEMO, in collaboration with a GFMI OEM, published a study demonstrating that GFMI can effectively suppress a real sub-synchronous oscillation phenomenon observed in a remote area of the system [68], thereby presenting an alternative solution to the one documented in [25]. Based on these findings and similar analyses from Australia [69], the provision of positive damping for oscillations in power systems that are sensitive to system strength has been also deemed as a *core* capability for GFMI [7].

b) ERCOT experience: to maintain reliable PEIR operations, especially under low system strength conditions, two SC (175 MVA each) were implemented in the Panhandle region in 2018. In response to the substantial growth of PEIR (≈40 GW) in west Texas, approval was granted in 2023 for additional SC at six locations, providing a total capacity of 2100 MVA. Ongoing studies are focusing on identifying the most viable and effective enhancements for the ERCOT grid, including the integration of GFMI. An ERCOT-wide assessment has highlighted several benefits of GFM BESS on the grid [70]. Consequently, GFM performance requirements are currently under development and are expected to be released by 2024.

c) RTE experience: RTE has actively participated in multiple research initiatives on GFM over the last decade. After the MIGRATE H2020 project, RTE coordinated OSMOSE. Within the WP3, two 1-MVA-sized GFM BESS demonstrators were deployed in collaboration with an OEM and the École Polytechnique Fédérale de Lausanne (EPFL) [63]. Factory Acceptance Tests (FAT) based on a Power Hardware-In-The-Loop (PHIL) test bench have provided valuable insights into the ongoing development of GFM requirements. Four types of GFM capability, each with increasing requirements, were defined to account for the physical constraints of different resources, including overcurrent capability and available energy buffer. Currently, RTE is involved in the AGISTIN project to demonstrate the provision of GFM capability by loads [71].

3) Brief consideration on system restoration: GFM does not imply black start capability. The latter requires the unit to self-energize (automatic startup of the auxiliary loads), initiate a blacked-out grid, and sustain its operation for a specific duration. It also necessitates storage or an available primary source, along with several additional control layers. However, GFM does entail islanding capability, which facilitates restoration. Units with GFM could remain energized and ready to take on load, contributing to voltage support, while only dispatchable sources are expected to participate in the balancing task.

In conclusion, addressing the urgent need for GFM devices requires a combination of measures. This includes updating connection codes to require technical capabilities from grid users, developing new services when applicable, and programming investments in TSOs-owned assets when necessary. Considering the time required for grid code updates to take effect, the latter two solutions have been more immediately available. Notably, regions such as Texas, Australia, Italy, and Finland have opted for SC to ensure power system security. Meanwhile, solutions based on GFM BESS have proven to be more cost-effective in specific scenarios [72]. Lastly, Germany has embraced the installation of a new family of FACTS, capable of providing GFM capability, such as the E-STATCOM (where the *E* stands for Energy) [73].

While this section may not unveil groundbreaking revelations, its objective was to establish the foundation for nuanced discussions on the potential role of PEIR in providing GFM capabilities to meet evolving system needs. Additionally, we aimed to offer insights into the challenges that lie ahead.

III. Specifying GFM capability

Different sets of technical requirements specifying the expected behaviour of GFM resources have been proposed by various TSOs. NG ESO was the first to formalize them in the grid code framework as a non-mandatory requirement and has recently shared lessons learned from this exercise [5] and implemented an update. Similarly, AEMO published a Voluntary Specification for GFMI in 2023 [7]. These efforts have more recently been complemented by implementation guidance with more details about compliance verification, including testing benchmarks [74], [75]. In CE, a first standard was released in Germany [76], and an update of the Requirements for Generators (RfG) regulation has been submitted by Agency for the Cooperation of Energy Regulators (ACER) to the European Commission (EC), including mandatory GFM capability for PPM [6]. Other relevant contributions worth mentioning include [77], [78]. Finally, a dedicated ENTSO-E working group is addressing the particular case of HVDC-connected PPM [79], and the InterOPERA project has extended the analyses to Multi-terminal Multi-vendor DC grids [80]. In this section, we recall the main features of three of these examples while highlighting their similarities and specificities.

A. GB GFM code (GC013)

In 2022 NG ESO implemented the Minimum Specifications Required for Provision of GB GFM capability including:

- Active RoCoF Response Power: the transient injection or absorption of active power to the total system as a result of the RoCoF value at the PCC.
- Active Phase Jump Power: the transient injection or absorption of active power to the total system as a result of changes in the phase angle between the internal voltage source and the PCC.
- Active Damping Power: naturally injected or absorbed to reduce active power oscillations in the total system. Damped response of a GFM plant to an oscillation between the internal voltage source and the PCC.
- Voltage Jump Reactive Power: the transient reactive power injected or absorbed from the plant to the total system as a result of either a step or ramp change in the difference between the voltage magnitude and/or phase of the internal voltage source and the PCC.
- FFCI: reactive current injection that starts to be delivered into the system in less than 5 ms when the voltage falls below 90% of the nominal value at PCC.

B. AEMO' Voluntary Specification for GFMI

It was developed to provide initial guidance to stakeholders, including developers and OEMs, for the elaboration of GFM offerings considering the evolving regulatory landscape of GFM technology. Additionally, it is designed to contribute to future developments concerning technical prerequisites, standards, service specifications, and procurement procedures. This initiative was mandated by the AEMO's Engineering Framework Priority Actions publication [81] after the need was identified in [82], and is the result of a collaborative effort.

AEMO' Voluntary Specification defines GFMI as the capability to *maintain a constant internal voltage phasor in a short time frame, with the magnitude and frequency set locally by the inverter, thereby allowing immediate response to a change in the external grid*. Then, this document divides technical capabilities into two categories: *Core* Capabilities and *Additional* Capabilities, as follows:

- Core Capabilities are fundamental requirements for GFMI, ensuring basic operational effectiveness and grid stability. These include essential functions such as voltage source behaviour and frequency domain response.
- Additional Capabilities enhance the PEIR performance and adaptability in various grid conditions and needs. These advanced features focus on aspects such as improved interoperability and control functionalities.

The primary distinction lies in the level of necessity; Core Capabilities are crucial for fundamental operation, while Additional Capabilities provide extended functionalities for more complex grid scenarios. Moreover, achieving core capabilities is expected with minimal to no modification to plant hardware and operational processes compared to a Gfl design, whereas additional capabilities may involve hardware upgrades. However, GFM devices are expected to inherently possess some form of small energy buffer to achieve core capabilities, even if this energy buffer is not always available.

AEMO's voluntary specification also outlines the core capabilities that PEIR must possess to qualify as GFMI and, whenever feasible, presents anticipated performance descriptions for such inverters, in a qualitative manner. They include:

- Voltage Source Behaviour: GFMI should behave like a voltage source behind an impedance, maintaining a near-constant voltage magnitude and phase angle during transients, essential for instant power response during disturbances.
- Frequency Domain Response: GFMI should exhibit low impedance magnitude around the fundamental power system frequency, reflecting voltage source behaviour.
- Inertial Response: GFMI should provide a synthetic inertial response, offering *immediate* active power response to grid disturbances.
- Surviving Loss of Synchronous Connection: GFMI must operate stably in a grid lacking other GFMI or SM, adapting to changes like system splits or loss of SG.
- Weak Grid Operation and System Strength Support: GFMI should operate stably in weak grid areas, improving nearby Gfl PEIR stability and providing system strength support.
- Oscillation Damping: GFMI should adequately damp active and reactive power outputs following disturbances and contribute positively to damping oscillations in the sub-synchronous frequency range.

AEMO's voluntary specification illustrates the expected response of GFMI under various conditions, emphasizing stability and responsiveness associated with core capabilities.

The deliberate omission of detailed quantitative requirements aimed for flexibility to accommodate the evolving industry expectations and system needs. More recently, AEMO collaborated with industry stakeholders and consultants to develop a simulation-based test framework to demonstrate GFMI capability as per the voluntary specification [75].

C. ENTSO-E CNC

In Europe, the RfG CNC is, at the time of writing, under revision. The proposed draft introduces non-exhaustive GFM requirements as follows: *within its current and energy limits, the PPM shall be capable of behaving at the terminals of the individual unit(s) as a voltage source behind an internal impedance (Thevenin Source), during normal operating conditions and upon inception of a network disturbance* [6].

The system response is further specified for network disturbances, as long as the installation limits are not reached: *the instantaneous AC voltage characteristics of the internal Thevenin source shall be capable of not changing its amplitude and voltage phase angle while positive sequence voltage phase angle steps or voltage magnitude steps are occurring at the connection point. The current exchanged between the PPM and the network shall flow naturally according to the main generating plant and converter impedances and the voltage difference between the internal Thevenin source and the voltage at the connection point*.

As for AEMO, detailed dynamic performances are excluded. They will be defined at the national level by relevant System Operators (SO), helped by non binding recommendations from Implementation Guidance Document (IGD) to be issued next year (2025). Finally, ongoing efforts at the normalization level should facilitate compliance verification in the years to come, specially for PPM connected to the Low Voltage (LV) and Medium Voltage (MV) distribution networks [76], [83].

It is nonetheless clearly stated that the installation *shall be capable of stable operation when reaching the PPM current limits, without interruption, in a continuous manner and returning to the behaviour described before as soon as the limitations are no longer active. If reaching the current limit, the GFM behaviour must be maintained for responses as specified before for disturbances that require the current to vary in the opposite direction of the active limitation.*

Moreover, for type A units (in France below 1 MW) the requirement is optional and is defined up to the PPM *inherent energy storage*, which means *an energy reserve available in physical components of a PPM, which has not necessarily been designed to suit the grid forming requirements, but may be used for such purposes, without affecting the design of the physical components of individual units*. From type B units (P_{max} >1 MW) the requirement will become mandatory and include an inertia consideration as *contributing to limiting the transient frequency deviation* for over frequency events, extended to low frequency only for electricity storage module, but also for Type C and D PPM (P_{max} >18 MW in France). In those cases, the relevant SO is allowed to request the provision of additional energy beyond the inherent storage.

D. Discussion on different requirement sets

A consistent trend in the different definitions of the GFM capability is the requirement of a Voltage Source Behaviour characterized by the capability to maintain a *constant* internal voltage (in amplitude, phase, and frequency) behind a (constant) internal impedance during transients [84]. Whether explicitly stated or not, the *internal voltage phasor* (and/or impedance) of GFMI is allowed to change on a longer time scale to achieve desired performances, typically synchronization, positive damping, power reference tracking and limitation due to physical constraints. Additional requirements on the output active and reactive power and/or current in response to variations in voltage amplitude, phase, frequency, or grid-side impedance at PCC are ways to quantify this behaviour.

To ensure clarity, following the lessons learned from NG, it is recommended to explicitly delineate detailed performance requirements for scenarios in which resource technical limits are reached and those in which they are not. While current limits are well understood by multiple stakeholders, a challenge remains in the unambiguous definition of *inherent* energy limits and how they may evolve with operating conditions, a characteristic closely tied to the underlying technology.

Importantly, the term GFM includes both generating and non-generating devices, irrespective of whether they are connected to the transmission or distribution networks. Further work may still be required to assess the impact of GFM behaviour on Distribution System Operators (DSOs) operational practices, a topic beyond the scope of this paper.

IV. Providing GFM capability with BESS

BESSs have been identified as the low-hanging fruits of the GFM capability tree [85] with GB and Australia leading the harvest [72]. Finland may follow after requiring GFM capability for all BESS connected in areas with a high penetration of PEIR [86]. In this section, we share Zenobē Energy experience with GFM BESS projects under the framework of the SP2, where three contracts were secured in Blackhillock, Kilmarnock South, and Eccles. These sites provide the stability services addition to active and reactive power services, hence as one of multiple revenue streams [87].

The Kilmarnock South project is a 300 MW/600 MWh BESS project with a GFMI solution. The site is directly connected to the 400 kV transmission system and consists of 102 GFMI and MV Power Stations, 445 modular energy storage solutions, and step up to 400 kV through the HV transformers. Each inverter specifies its GFM capability, and the power plant controller aggregates each response. Since the site was originally designed to be 200 MW based on 220 MVA, the following simulations use them as base values.

The site is designed to maximize the SCL and inertia provisions by utilizing the short-time overloading capability of element, including inverter, battery module, and balance of plant. The site has achieved 2.1 pu of SCL (corresponding to 460 MVA) and 0.3 pu of inertia power (60 MW, base 200 MW, equivalent to 1.500 MVAs) for all operational conditions, as demonstrated by EMT simulations.

a) Monitoring infrastructure: a Dynamic System Monitoring (DSM) with a sampling rate of 1.6 kHz to 25.6 kHz has been installed at PCC to verify inertial response and FFCI within 5 ms upon inception of disturbance events, which can be triggered by RoCoF, voltage and/or phase angle changes.

b) Demonstrating inertial response: as illustrated in Fig. 4, EMT simulation consistently demonstrated inertial response to different RoCoF events under all operational conditions (full discharge, full charge, idling). Inertia constant and damping factor are adjusted accordingly.

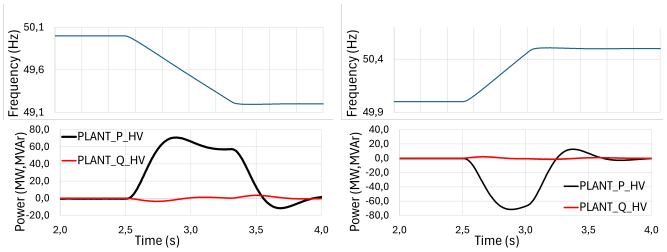

Fig. 4: Frequency drop/rise of 0.8 Hz at 1.0Hz/s

c) Contribution to SCL: EMT simulations demonstrated in excess of 2.0 pu fault current at the required PCC retained voltage, and enhanced fault current characteristics for remote faults due to the prolonged current injection. While a SC exhibits higher peak fault current, it may also experience a faster decay. Given that the SCL contribution is assessed at 100 ms after the fault, the response offered by the GFMI can be made comparable to the SC for a moderated rating increase as shown in Fig. 5.

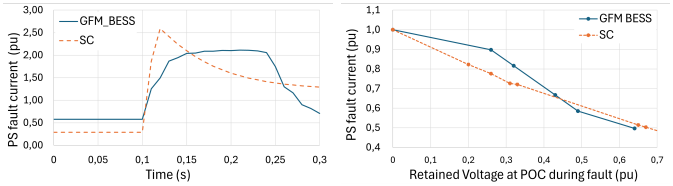

Fig. 5: 3ph-gnd fault with PCC retained voltage of 0.26 pu.

d) FAT: towards commercial operation, real model-based tests with individual GFMI and Hardware-In-The-Loop (HIL) tests on multiple GFMI have validated the provision of GFMI capabilities. These tests include:

- Active RoCoF Response Power: Demonstrate contracted Active RoCoF Response Power considering any stacking with other active power services under BESS's charging/ discharging status.
- Active Phase Jump Power: Demonstrate the response to a phase jump of 5 degrees/ 60 degrees injected at GFMI terminal and PCC in the HIL simulator without trip.
- Faulted Condition Contribution (FRT, FFCI): Demonstrate the contracted SCL during the fault conditions, and the active phase jump power, FRT and FFCI capabilities.
- POD: Respond to the voltage and frequency oscillations within the sub-synchronous frequency range, for the power oscillation frequency of 5 Hz, 7 Hz and 9 Hz.

V. Impact of GFM requirements on HVDC Control

While providing a great increased flexibility in control, grid forming via HVDC also introduces a new feature in the power system. It is in this context important to recall that the HVDC is a transmission system and not a generating unit nor a storage. The sections below will discuss the physical and operational constraints of the HVDC and when the HVDC will inherently give a different behavior than a synchronous machine. If the constraints of the HVDC are not reflected in the requirement specifications, it may be impossible to fulfill the requirements. Also, there is a risk for contradictory requirements that need to be considered, see [88]. The following items are discussed and illustrated with simulations:

- Impact of virtual inertia
- DC side and grid forming control
- Transient current capability
- Virtual impedance impact on large power disturbances
- Synchronization

In the simulations, a generic controller was used for balancing the arm voltages. This means that although realistic, the performance will differ from that of a fully optimized vendor model. However, the level of detail in the model is the same, and the same general tendencies can be observed. The simulations are performed using a symmetric monopole point to point HVDC setup with power directions according to Figure 6. Station 1 is inverter in active power control (grid forming) while station 2 is rectifier in DC voltage control mode in all simulations except for in an offshore case. In all simulations, negative sign of active power means rectifier operation and positive sign means inverter operation. In the figure, each cell represents a half-bridge submodule.

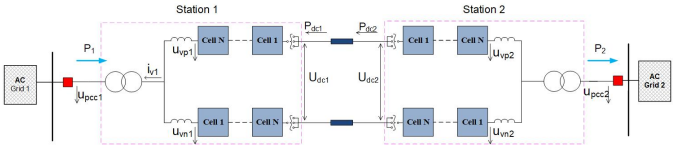

Fig. 6: Simulation setup.

A. Impact of virtual inertia

To resemble the behavior of the synchronous machine, it is common that grid forming methods implement a virtual inertia via, for instance the swing equations. This will slow down the internal voltage angle during disturbances. Compared to the synchronous machine with a physical inertia, some fundamental differences exist. For instance, a large inertia may be desirable from a frequency support point of view but may severely contradict other requirements posed on the HVDC. The larger the emulated inertia, the larger the required energy requirement for grid frequency support. For the synchronous generator, the inertia stems from a large spinning energy. In a VSC HVDC, no such energy is available since the energy stored on the DC side is very limited and must be available for AC voltage generation, [89]. Thus, the remote station AC network must provide the energy for grid support. As a consequence, the remote AC grid must in this case be able to handle transient power variations. Even so, the energy transmission capability of the link itself is limited. In principle, a separate external energy storage could also be used for grid support. However, such storage will increase the design cost and is at the time of publication not commercially available. If the energy can be provided from the other side or via a separate storage, it is possible to provide a large inertia at least in the active power controlling station. The larger the inertia, the larger the energy transfer on the link during large disturbances will be. A case where active power will be largely affected directly by inertia is RoCoF. An example is given in Figure 7 where the grid frequency in the active power controlling station 1 operating as inverter is ramped down from 50 to 49 Hz with the rate 2.5 Hz/s. The upper plot in Figure 7 shows the response in active power in the active power controlling station 1 for different inertia constants H. Also, a frequency controller with dead-band was employed. It can be seen that due to the slower change of voltage angle following with high inertia, the active power response in station 1 is larger with higher inertia and also that the overshoot is larger with higher H. As also further discussed below, the larger the inertia, the larger the impact on the DC voltage will be due to this. The lower plot in Figure 7 shows the corresponding response in active power in the DC voltage controlling station 2 which is in grid following control. From Figure 7 it is also clear that in order to be able to provide the frequency support, some headroom is needed in the design. The larger the inertia in station 1, the larger the corresponding active power change response by the DC voltage controller in station 2 will be in order to balance the DC voltage on the link. This emphasizes the need for a sufficiently fast DC voltage control when the inertia is high in the other station. The AC network connected to DC voltage controlling station must also be able to accommodate this rather large power variation.

An example of a severe power disturbance is a large voltage phase jump in the grid. Assuming that the grid and internal converter voltages are 1 pu, the instantaneous change in active power caused by a phase jump is given by (2). Here, ΔP_δ is the change in active power, X_{conv} is the converter impedance (including converter transformer), SCR is the short-circuit current ratio. It can be seen that the instantaneous change in power is proportional to the angular voltage change, thus inertia has a negligible impact on the magnitude of power change. The level of inertia will however be reflected in the recovery phase after the disturbance.

$$\Delta P_\delta \approx \frac{1}{X_{conv} + \frac{1}{SCR}} \sin(\Delta\delta) \tag{2}$$

This is illustrated in Figure 8a-8b. Here, a positive phase jump of 10 degrees is applied for five different virtual inertia values in station 1 which is in active power control. Figure 8a shows the response of station 1. The corresponding response of Station 2 which is in DC voltage control is shown in Figure 8b.

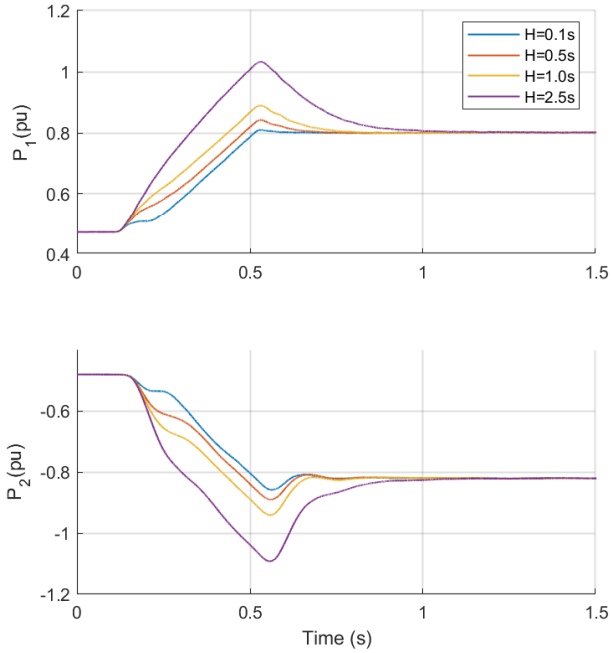

Fig. 7: Response in active power to a frequency ramp 2.5 Hz/s for different inertia in active power controlling station 1. Upper plot shows the active power in station 1. Lower plot shows active power in station 2

The initial impact on the active power in station 1 is roughly the same for all cases. In the recovery phase, recovery to pre-fault value is affected significantly by the inertia. A higher inertia gives a longer lasting active power deviation in station 1 which is also reflected in the DC voltage controlling station 2. The higher the inertia in station 1, the larger is the impact on the DC voltage of the link and the larger the active power response in station 2 will need to be to counteract that. To be able to handle this, as also further discussed in section V-B, the DC voltage control in the remote station must then be sufficiently fast to respond not to compromise DC voltage stability. Thus, an inertia requirement in the active power controlling station will also stress the DC voltage control in the other station.

Since a virtual inertia slows down the voltage angle change of the converter, it will also slow down the active power response time resulting in slow step responses in active power. This is illustrated in Figure 9. For the same reason, slow recovery time after faults in the AC networks in the active power controlling station results. The impact on fault ride through behavior and some fast-acting control will increase with higher inertia.

B. DC side and grid forming control

The implementation of grid forming control as a voltage source behind impedance is also possible in the DC voltage controlling station. This can be beneficial for weak grids as

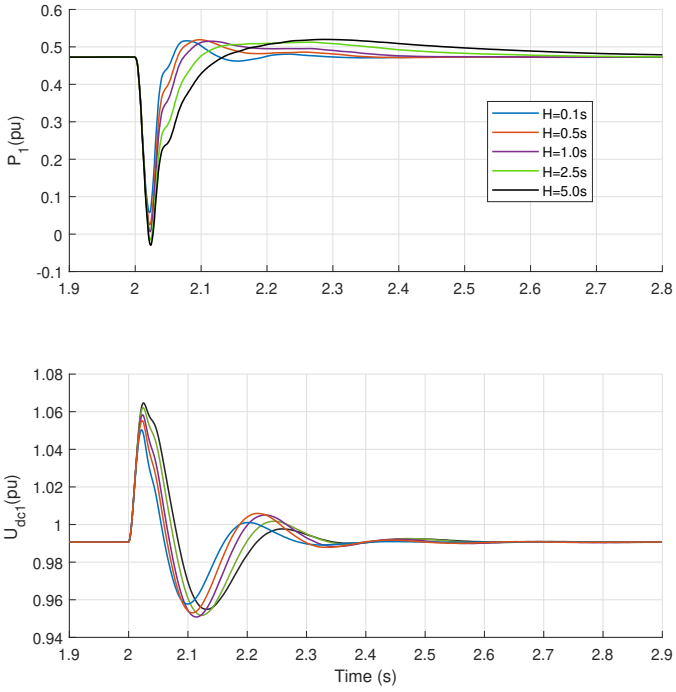

Fig. 8a: Station 1, upper plot active power P_1, lower plot DC voltage, station 1 in active power control

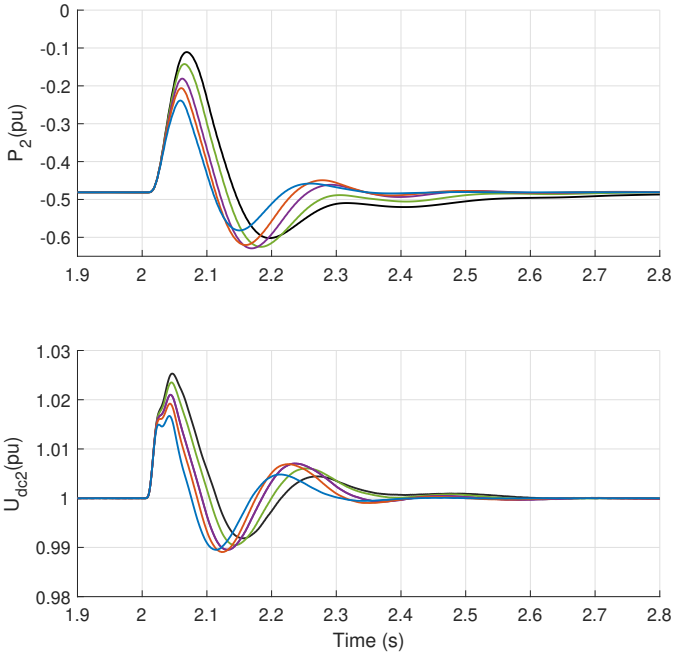

Fig. 8b: Station 2, upper plot active power P_2, lower plot DC voltage, station 2 in DC voltage control

shown in [90]. It should be noted that ”inertia” for dc voltage control in this case does not resemble a true inertia as in active power control station i.e. it is just a measure of stiffness so that a less stiff response (fast dc voltage control) resembles low H and a more stiff response (slow dc voltage control) resembles high H. Just as in the active power controlling

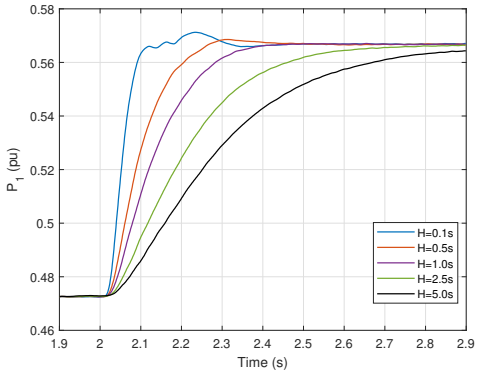

Fig. 9: Step response in active power for different inertia, H

station, see Figure 9, an inertia requirement in the DC voltage controlling station will slow down the response of the voltage angle and thus result in a slower change in active power flow. This in turn will slow down and thus possibly deteriorate the DC voltage control, see also [91]. Any such requirement must thus be thoroughly investigated and handled with great care. A simultaneous inertia requirement in the active power controlling station will also further increase the strain on DC voltage stability since as discussed above in the previous section, a disturbance in the active power controlling station may then create an energy transfer requiring a fast response from the DC voltage controlling station. This emphasizes that an important limiting factor is related to the relatively low energy capability of the link and the bandwidth limitations of the DC voltage controller. This is often overlooked since it is not directly related to AC side behavior but rather to the internal HVDC control and design. For certain disturbances, for instance large phase jump or severe inverter AC faults, energy may accumulate on the DC side, which for an MMC converter will also transiently increase the submodule capacitor voltages. This could affect the continued operation of the link depending on the severity of the disturbance and the HVDC topology. This also further emphasizes the need for sufficiently fast DC voltage control. Another disturbance that could be more critical for grid forming schemes for the same reason is large temporary temporary over voltage. To illustrate the discussion in this section, Figure 10 shows an example of an HVDC-link experiencing a 3-phase fault near station 1 which is in active power control operating as inverter. The connected AC grids on both stations are relatively weak. In the DC voltage controlling station 2 operating as rectifier in grid forming operation, one fast DC voltage controller corresponding to lower inertia and one slow DC voltage controller corresponding to a higher inertia is considered. It is seen that in the slow response case corresponding to higher inertia, the DC voltage controlling station is more sensitive to the fault in the other station due to the slower DC voltage control. Thus, it will not be possible for the DC link to recover after this disturbance if the DC voltage controlling station has higher inertia than feasible, as the control cannot react fast enough to keep the voltage below admissible levels. As explained above, this impact is due to slowing down the change in AC voltage angle. The very same behaviour can be expected if the same fault is here applied at the terminal of DC voltage control station instead if active power control is slow due to high inertia constants. For faults close to the rectifier, the converter may instead go into over-modulation, i.e., lose control due to low DC voltage if the DC voltage can not be controlled fast enough by the remote station.

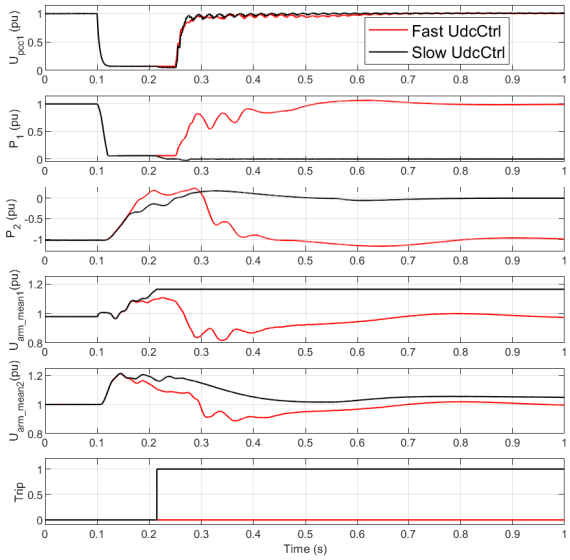

Fig. 10: Example of response to three phase fault in active power controlling station 1 for different speed of DC voltage control in the DC voltage controlling station 2.

An aspect of modelling which is often not accounted for, since the focus is on the AC system response, is the internal dynamics on the DC side of the HVDC link. A large disturbance on the AC side will cause a disturbance also on the DC side. To investigate the impact, the DC side and the corresponding control system consisting of DC voltage control as well as energy balancing controllers for the converter arms would need to be modeled. For grid forming converters, this may be of extra importance since an inertia requirement as discussed in the previous section will slow down the converter output voltage angle and thus the DC voltage dynamics. For this reason, it could also be important to model the other station in the same detailed manner, especially if there is an inertia requirement in both stations, since the dynamics of both stations as discussed will affect the DC voltage stability. As shown in section V-D events like large voltage phase jumps (depending on jump magnitude and grid strength) may even pose a challenge in controlling MMC energy or submodule capacitor voltages, which is overlooked if a simplified model is used. In the same way, a situation as depicted in Figure 10 would be difficult to evaluate without

a detailed representation of the DC side. There is a direct connection between the different requirements on an HVDC link and the physical design, and thus to the design cost. In a case where the purpose is to determine that a design is not only technically, but also economically feasible a detailed model representation of the DC side as described above is needed.

The following example considers grid forming capability of DC voltage control in an HVDC connecting Power Park Modules (PPM's). An HVDC converter can have islanded operation capability only if there is another supporting station that controls the DC voltage in a stable manner. Figure 11 shows a case where gridfollowing wind turbines are connected to an offshore converter controlling the voltage and frequency offshore as is traditionally done, thus acting as a slack bus for offshore power. This means that the offshore converter can be considered as a constant power source not contributing to DC voltage control. As a consequence, DC voltage stability must be ensured via DC voltage control in the onshore station. If grid forming behavior in terms of inertia is required by the onshore converter to supply/absorb the active power required by the AC grid depending on the type of transient events, there will be a conflict between maintaining the DC voltage stability and grid forming behavior since the DC voltage control will be slowed down. In the example in Figure 11, P_1 is the active power in onshore converter, P_2 is the active power in offshore converter, U_{DC1} and U_{DC2} are the DC voltages of onshore and offshore converter respectively and δ_1 is the grid phase angle of the onshore grid. At t =0.1 s, a 10 degree negative phase jump occurs. The active power infeed from offshore converter remains constant throughout the disturbance period. This means that the energy fed to onshore in the phase jump comes from the converter submodule capacitance and cable capacitance and the DC voltage starts to fall quickly. Soon after that, the DC voltage control in the onshore converter reacts to restore the DC voltage by taking the energy from the onshore grid until pre-fault values are reached. When grid phase angle at $t = 0.9$ s experiences a positive phase jump back to 0 degrees, the DC voltage instead increases meaning the energy in submodule capacitance and cable capacitance increase. Had the DC control reacted slower to the first disturbance (as would have been the case with a higher inertia), the DC voltage would have decreased more and there would have been a risk to compromise the DC voltage stability. This will always be the case if the other converter is in control of frequency and voltage not contributing to DC voltage control. In principle, similar behavior is expected also if the remote station is in active power control mode.

C. Transient current capability

A VSC cannot tolerate transient overcurrent levels comparable to those of a synchronous machine. It normally has an impedance smaller than that of the synchronous machine and less current capacity. Further, during the fault and the following fault quasi steady state, the fault current provision is

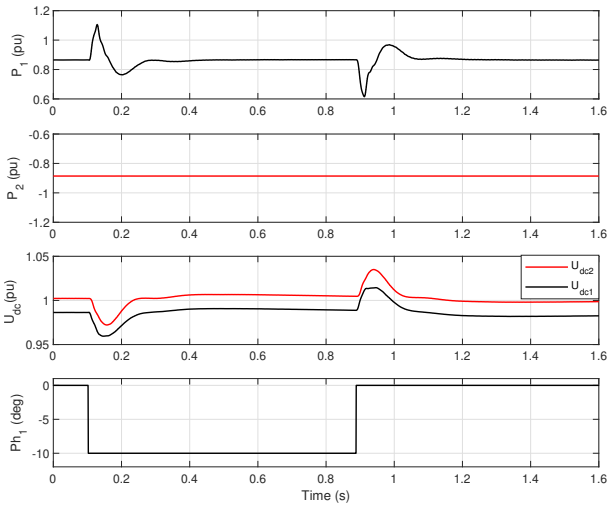

Fig. 11: Example of response to 10 degree phase jumps in onshore grid.

limited to one per unit or slightly above that. It is important to note that this is the total current, including both positive and negative sequence. It could thus be necessary to determine how to prioritize between positive and negative sequence fault current provision from the converter. When the transient current is limited in the VSC, it will affect the behavior for large disturbances which will then deviate from that of a synchronous machine. Any grid forming implementation must thus be equipped with a scheme to limit transient overcurrent in order to guarantee continued operation. If the implementation includes an inherent current controller, this is trivial. If a pure voltage source emulation (VSE) scheme without underlying current control is implemented, this must be performed by other means. One possibility is to do a hard mode shift to current control when the disturbance is detected. Other possibilities include current limiters in parallel to the VSE scheme. Note that with a properly implemented current limitation scheme, the current level for a grid fault should not be critical itself. Still, the transient current during a disturbance could be critical in the sense that the DC side voltage or submodule capacitor voltages are charged to a critical level. To further improve current limitation, a virtual impedance or admittance via introducing an artificial voltage drop in the converter may be implemented. This could be crucial to increase the withstand capability, see V-D, and also to improve damping.

D. Virtual impedance impact on large power disturbances

For large power disturbances (e.g., large phase jumps), a gridforming converter will behave differently from a gridfollowing converter since the voltage angle of the grid forming converter will not follow the grid voltage angle as quickly. The instantaneous change in active power is given by (2). It is seen from the equation that the larger the total converter impedance X_{conv} including the virtual impedance, the less the corresponding instantaneous change in active power will

be. Thus, in the grid forming converter, implementation of a virtual impedance or admittance as mentioned in the previous section could be necessary for withstand. Figure 12a shows such an example for a 30 degree positive phasejump in a grid with SCR=20. The phase jump is applied in active power controlling station in cases with and without a virtual impedance implemented. The case without added virtual impedance trips while the case with virtual impedance withstands the large disturbance. A large positive phase jump during inverter operation when running close to full power and the grid is strong is anticipated to be the most critical case. In that case, the issue would be related to the DC over-voltage or submodule capacitor voltage caused by the rapid change of AC side active power. In the case without virtual impedance shown here, the power exceeds 1.5 pu. The virtual impedance helps in limiting the difference between DC and AC power and hence the charging of DC side energy and submodule capacitors. This is an example showing the importance of modeling the DC side dynamics in an MMC properly. Virtual impedance will help with improving performance for phase jump in both directions. Figure 12b shows the similar cases but for a 30 degree negative phasejump. Here, DC side charging is not as critical as in the positive phasejump case in Figure 12a. Current is hard limited in both cases, avoiding a trip. However, due to the less aggressive current limitation in the case utilizing a virtual impedance, the frequency support properties (visible in active power response) are better in that case in the sense that the frequency support is given faster.

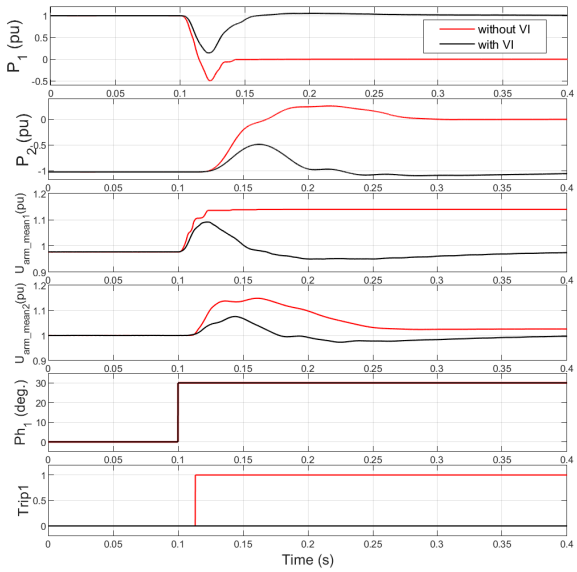

Fig. 12a: Positive phase jump of 30 degrees in active power controlling station 1, with and without virtual impedance (VI).

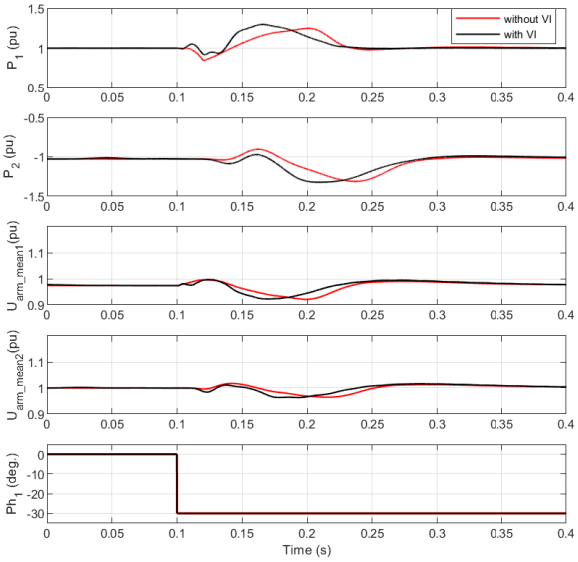

Fig. 12b: Negative phase jump of 30 degrees in active power controlling station 1, with and without virtual impedance (VI).

E. Synchronization

For a converter connected to a grid where other units can affect frequency and voltage, some grid synchronization method is necessary to handle disturbances where the converter goes into limitation. The literature describes both schemes with and without a phase-locked loop (PLL). A relatively fast continuous synchronization to the grid may improve the transient stability and possibility to resynchronize to the grid after large disturbances. Examples of such disturbances are large voltage angle jump or high RoCoF when converter operates at rated power. The conflict of the synchronization stability and the inertia response of the grid forming converter is discussed in [92], where a transient damping method (in which grid frequency is estimated using a PLL) is added in the active power control loop.

An important aspect related rather to steady state behaviour without any grid synchronization which may not be obvious is the power order tracking when frequency deviates from nominal, [93]. The deviation from the active power order may then not be acceptable for an HVDC. The deviation from the active power order for VSM in steady state without frequency synchronization can be understood from Figure 24 and the following discussion. With a reasonable choice of parameters, the power deviation for a 0.5 Hz frequency deviation from nominal frequency could be around 0.5 pu. which is large considering for instance a 1 GW link. In that case, an estimation of grid frequency via a PLL/FLL would be necessary to compensate for the frequency deviation to achieve proper power tracking.

Some simulation examples are shown in Figure 13. Here, a change in frequency from 50 to 50.2 Hz is applied. The different cases show synchronization with different time constants of a PLL used for synchronization. In the case with no synchronization a large (0.1 pu.) deviation in active power remains in steady state after the frequency change. Although

coherent with gridforming properties, such a large deviation from the power reference might not be desirable. It should be noted that, besides the use for reference following and resynchronization after disturbances, a PLL is traditionally also used for synchronization to grid before deblocking the converter. In some papers, e.g. [94], it is claimed that it is possible to synchronize to grid before connection to grid without using a PLL. However, in many applications (HVDC/FACTS) such a solution is not feasible as it assumes that there is already an established DC voltage before energizing the converter.

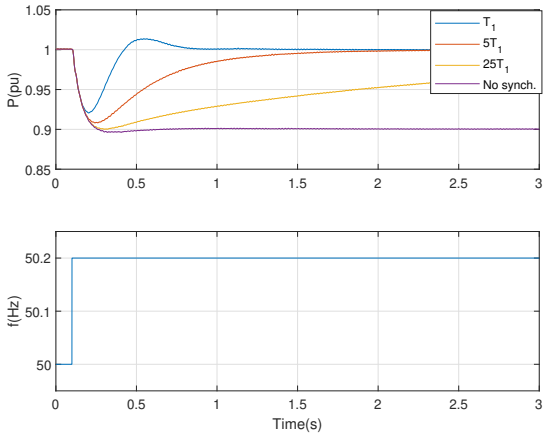

Fig. 13: Example of active power response with different synchronization speed to a grid frequency change from 50 to 50.2 Hz.

VI. Towards a comprehensive modeling of grid forming control

The evolution of the power system has been outlined in previous sections. New rules are being incorporated to grid codes and, among them, notably those dealing with the GFM capability. On the manufacturer side, providing solutions with such capabilities has important implications, as also described in previous sections.
In addition to this industrial challenge, a twofold theoretical challenge has to be tackled: provide a definition of grid forming control and establish a coherent theoretical framework around this concept. Over the last years, numerous types of grid forming control schemes have been proposed in the literature, which has led to a somewhat complex landscape.
The aim of this section is to offer a consistent framework of study for the various types of grid forming control, starting from basic concepts. This requires to clarify the model of the system under control, propose a rigorous procedure leading to various topologies of controls, some few variants and eventually design the parameters of the controllers.

The proposed material will mainly focus on transmission grid connected converters. It is organised as follows:

- Bibliographic review of a selection of key papers addressing grid forming control
- Identification of the dynamic model of the system
- Design of the active power control
- Enhancement of large-disturbance stability
- Small-signal stability analysis in a wide range of grid strength
- Proposal of a 4 VSCs benchmark to illustrate previous insights on a more complex system.

A. Short bibliographic review on grid forming control

Different solutions have been proposed to control the active power exchanged between the converter and the AC grid with controlled voltage angle which is the fundamental principle of the grid forming control. Among them, the droop control-based [95] is one of the most well-known solution. The frequency of the modulated voltage is calculated from a difference between the power reference and the power measurement. It can be demonstrated that a frequency droop control is naturally integrated in this type of control. When the participation to primary frequency regulation service is not required, it is possible to incorporate an estimation of the grid frequency into this control scheme [96] to ensure reference tracking in steady state. Various control structures aim to emulate the synchronous generator like the Virtual synchronous machine [97] [98], Synchronverter [99], Inducverter [100], Virtual induction machine [100]. With a Proportional Integrator (PI) controller [101], the grid forming control is also providing some inertial effect without using any information on the grid frequency. The matching control [102] is based on an analogy between the capacitor of the DC bus and the inertia of the synchronous machine. The virtual oscillators has been introduced in order to facilitate the self synchronisation [103]. In [104], the authors improve the power reference tracking capability of a grid forming control thanks to a feed-forward action on the angle.

In addition, the regular presence of an LC or LCL filter on the AC side of a VSC also requires to be managed by the control scheme as it brings additional dynamics to the converter. A possible solution is to implement a cascaded voltage-current loops [105], [106]. The optimal design of the current and voltage controllers are not straightforward. In [105] a tuning approach based on the optimization of the placement of eigenvalues is used. In [107], a specific Model Predictive Control to design the voltage and current controller is used. Alternative options for designing these controllers can be found in [108], [109]. Additionally, it is possible to achieve direct voltage control, which is a simpler solution requiring less tuning effort [96]. Consequently, the multitude of grid forming control schemes, especially the diverse names assigned to controllers with essentially similar characteristics, contributes to confusion among engineers and researchers.

Several reviews on grid-forming control can be found in the literature [110]–[112]. However, to the best of the authors' knowledge, none of these reviews delve into the fundamental principles required to unify and design the various types of grid forming control.

B. Definition of the model for the design of the power synchronisation control

Before starting to design this control, it is highly important to clearly define the model of the system to be controlled.

Firstly the model of the converter must be specified. The main function of the VSCs is to modulate the DC bus voltage in order to generate a set of three-phase voltages $v_m = (v_{m_a}, v_{m_b}, v_{m_c})$ as shown in Fig. 14a. This requires defining a set of three-phase signals in the control $v_m^* = (v_{m_a}^*, v_{m_b}^*, v_{m_c}^*)$. The low-level control, which manages the transistors switching, aims to ensure that the average value of the phase voltages over the transistor switching time T_s is equal to their corresponding control signals:

$$< v_{m_j} >_{T_s} = v_{m_j}^*, \quad j = \{a, b, c\} \tag{3}$$

Hence, in a first approximation, the VSC can be assimilated to an ideal three phase voltage source that is driven by the control as sketched in Fig. 14b. In other words, the converter is represented by a lossless power amplifier between a signal generated by the control v_m^* and the actual modulated three-phase voltages v_m. The dynamics of transistor switching can be approximated by a delay that takes into account the internal operation of the converter.

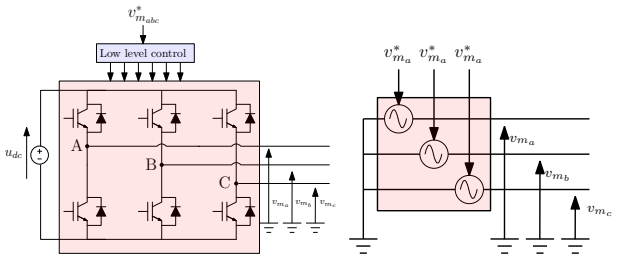

(a) Full model (b) Average model

Fig. 14: Basic representation of a Voltage Source Converter

Secondly, the grid connected to the converter has to be modeled. As shown in Fig. 15, the converter is assumed to be connected to a Thévenin equivalent system composed of a voltage source v_e in series with the grid inductance L_g. To simplify the analysis, the grid resistance is neglected, without loss of generality. On the converter side, a lossless connection is also considered in the form of an inductance L_c. With a proper choice of per unit system, the transformer can be represented by merely its leakage inductance.

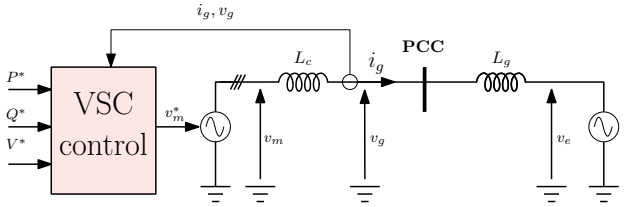

Fig. 15: Connection of a VSC to a Thévenin equivalent

In steady state, for a given grid frequency, it is possible to associate a phasor to each AC voltage according to:

$$\overline{V}_x = V_x \, e^{j(\delta_x)} \tag{4}$$

Similarly, a phasor can be associated to the current i_g flowing out of the VSC (see Fig. 15). Assuming that the current phasor lags the phasor of the Thévenin voltage source by an angle ϕ, the former can be written as:

$$\overline{I_g} = I_g \, e^{j(\delta_e - \phi)} \tag{5}$$

With this static formulation, the system can be represented by the electrical circuit shown in Fig. 16a with the corresponding phasor in Fig. 16b.

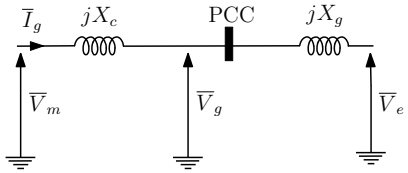

(a) electrical circuit representation

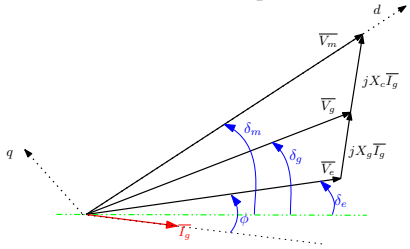

(b) phasor representation

Fig. 16: Static model of the system

From that circuit, two expressions are easily derived for the active power in terms of phase angle differences, namely:

$$P = \frac{V_m V_g}{X_c} \sin(\delta_m - \delta_g) \tag{6}$$

$$P = \frac{V_m V_e}{X_c + X_g} \sin(\delta_m - \delta_e) \tag{7}$$

From (6), it can be derived a first type of control [113]. In the sequel, only the second formulation of the power (9) is considered to design the control.

Getting back to time domain, a time-varying angle is associated to each angle in the phasor, according to:

$$\theta_x = \delta_x + \omega_b \, t \tag{8}$$

Substituting θ_m (resp. θ_e) to δ_m (resp. δ_e), Eq. (7) can be rewritten as:

$$P = \frac{V_m V_e}{X_c + X_g} \sin(\theta_m - \theta_e) \tag{9}$$

The VSC control is implemented in the well-known dq reference frame. The d axis is aligned with the phasor $\overline{V}_m$ of the modulated voltage v_m. Thus, in steady state:

$$v_{md} = V^*, v_{mq} = 0$$

Where V^* represents the voltage magnitude reference.

Since v_{md} and v_{mq} are generated by a controller, it is possible to modify these components in order to incorporate a "virtual reactance" X_v, according to:

$$v_{md} = V^* - X_v i_{g_q} \quad v_{mq} = X_v i_{g_d} \tag{10}$$

which are nothing but the steady-state equations of an reactance in series with the VSC and the Thévenin inductances. Its purpose has been presented in Section V-D to mitigate the effect on a phase shift on the power variation in the converter. With the latter, the model under consideration is hybrid, since it refers to both the physical components as in Fig. 15, and the virtual reactance, as shown in Fig. 17a. A virtual voltage $\overline{V}$ is also added in the model. Introducing δ as the phasor angle associated to this voltage, the active power expression is easily rewritten to take X_v into account:

$$P = \frac{VV_e}{X_v + X_c + X_g} \sin(\delta - \delta_e) \tag{11}$$

It is also possible to associate a time domain angle θ to δ, it yields:

$$P = \frac{VV_e}{X_v + X_c + X_g} \sin(\rho) \tag{12}$$

with the angle ρ defined as:

$$\rho = \theta - \theta_e = \delta - \delta_e \tag{13}$$

$\overline{V}$ is now taken as reference of the dq frame (see Fig. 17b). The active power control will be based on the phase angle difference $\delta - \delta_e$.

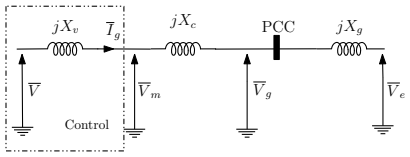

(a) electrical circuit representation

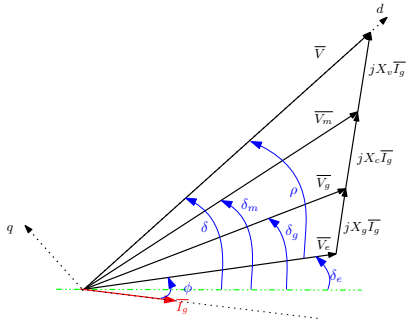

(b) phasor representation

Fig. 17: Static model extended to the virtual inductance

C. From a static model to a dynamic one

In order to design a control, a dynamic model is needed. The aim of this section is to explain why the static model derived in the previous section can be also used as a dynamic model for two different types of grid forming control including a current loop or not.

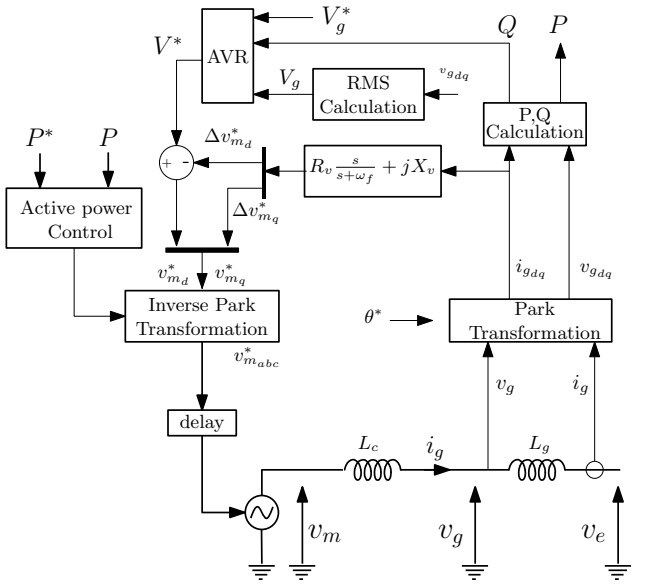

Fig. 18: Overall organisation of a Direct Voltage grid forming control

1) Direct voltage control: Fig. 18 shows the overall organisation of the first type of Grid Forming control. The symbol * is employed to designate a control reference, corresponding to its equivalent variable in the system.

The core element is the active power control which generate the angle θ^* of the time varying virtual voltage v^* associated to $\overline{V}$. Doing so, it can be understood that this loop is also synchronising the converter to the grid. This double functionality is summarized in a unique expression: the power synchronisation control. An Automatic Voltage Regulator (AVR) is controlling the voltage V_g at the Point of Common Coupling (PCC) (see Fig. 17a). More precisely, it generates the magnitude V^* of that virtual voltage. As previously explained, $v_{m_d}^*$ and $v_{m_q}^*$ are derived from V^* by possibly adding a virtual inductance. Since there is direct link between $v_{m_d}^*, v_{m_q}^*$ and V^*, this control can be called a Direct Control Grid Forming. It is also referred in the literature as a Voltage Control Grid ForMing (VC-GFM) control. This is the name that will be used in the following sections.

In ordre to identify the dynamic model, an open loop control is firstly considered to check its validity in dynamic conditions. Note that this type of control could not be used in a real application, only in simulation. By inverting Eq. (12) ρ^* can be obtained as a function of P^*. Assuming that both RMS voltages V_e and V are equal to 1 pu, and linearizing Eq. (12) yields:

$$\rho^* = (X_c + X_v + \tilde{X}_g)P^* \tag{14}$$

Using this equation requires to have an estimate ($\tilde{X}_g$) of the grid reactance X_g. In simulation, it is possible to set $\tilde{X}_g = X_g$

The inversion of Eq. (13) yields θ^* as a function of ρ^*:

$$\theta^* = \rho^* + \tilde{\theta}_e \tag{15}$$

which shows the need to know the voltage phase angle θ_e. During this identification stage, it is possible to set this angle equals to the Thevenin voltage angle. It yields in frequency domain:

$$\tilde{\theta}_e = \omega_b / s \tag{16}$$

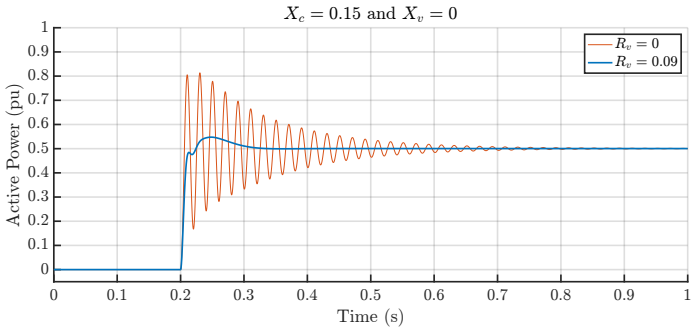

Fig. 19: Simulation of an open-loop control of active power

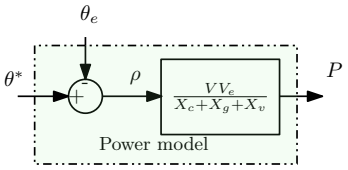

Fig. 20: Open-loop control of active power

As illustration, Fig. 19 presents simulation results obtained for a step change of 0.5 pu of P^* with a 0.15 pu connection reactance X_c. The grid is considered strong enough so that its reactance is negligible. It can be seen that the steady-state value of P is equal to 0.5 pu as expected, but the dynamic response unveils an oscillation at 50 Hz. The latter is due to the poorly damped poles of the grid (corresponding to the aperiodic variation of the current in the abc frame). As shown in [96], [114] they can be damped using a damping virtual resistance R_v as follows:

$$v^*_{m_d} = V^* - R_v \frac{s}{s+\omega_f} i_{g_d} \tag{17}$$

$$v^*_{m_q} = -R_v \frac{s}{s+\omega_f} i_{g_q} \tag{18}$$

in which the washout filter avoids affecting the steady-state voltage, while ω_f can be adjusted to obtain the desired dynamics. The response shown with blue curve in Fig. 19 has been obtained for $R_v = 0.09$ pu. If the required bandwidth on active power control is not too high, the small transient can be considered negligible and both the static and dynamic models can be considered equivalent. It can be concluded that the dynamic system can be represented by the simple block diagram shown in Fig. 20.

2) Introducing a current loop in the control: Traditionally, VSCs have been driven in grid-following mode, which is centered around a current control loop. To maintain the advantage of this control loop in terms of current limitation following a significant disturbance, certain grid-forming control schemes also keep the current control loop. In this case, the active power is still controlled by the voltage angle but the incorporation of current loops requires generating d, q reference currents which are coherent with the voltage angle generated by the active power control.

Those current references can be obtained from an estimation $\tilde{\overline{I}}$ of the grid current $\overline{I}$ using the difference between the voltages $\underline{V}$ and $\underline{V}_g$:

$$\tilde{\overline{I}}_g = \frac{(\overline{V} - \overline{V}_g)}{j(X_c + X_v)} \tag{19}$$

Decomposing this estimation into its d, q components yields:

$$\tilde{i}_{g_d} = -v_{g_q}/(X_c + X_v) \tag{20}$$

$$\tilde{i}_{g_q} = (V^* - v_{g_d})/(X_c + X_v) \tag{21}$$

The current references are set to the above estimated values, i.e.

$$i^*_{g_d} = -v_{gq}/(X_c + X_v) \tag{22}$$

$$i^*_{g_d} = (V^* - v_{gd})/(X_c + X_v) \tag{23}$$

Fig. 21 shows the corresponding blocks to be added. The left part deals with the generation of the d, q current references. It can be proved that a filter (with cut-off frequency ω_v) has to be applied to guarantee the stability of the system. The right part shows a current control loop similar to the one found in a grid-following control scheme. A simple proportional controller has been chosen (with gain $K_{p_{cc}}$) but a PI or even another controller is commonly used.

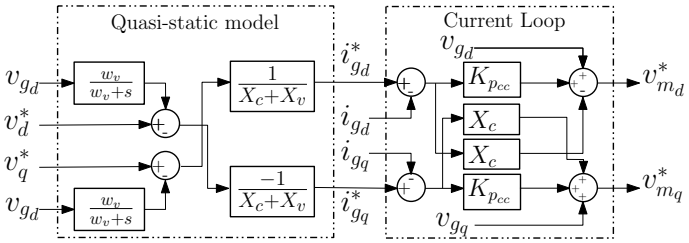

Fig. 21: Quasi static model and closed loop current control

The overall structure of grid forming control with current control loop is shown in Fig. 22. The active power control scheme is unchanged. No damping virtual resistance is needed for this control since the closed loop current control is already damping the grid modes.

By way of illustration, Fig. 23 presents simulation results obtained for a step change of 0.5 pu of P^*. The gain $K_{p_{cc}}$ has been set to yield a 3000 rad/s bandwidth for the system with current control loop. ω_v has been set to 100 rad/s. The corresponding response time is around $3/\omega_v = 30$ ms. The curves show that the responses with and without current control loop are quite similar; The steady-state value is the same, the dynamics are only slightly different. It can be concluded that the variant including the current control loop and the quasi static model can be represented by the same block diagram shown in Fig. 20. In the rest of the paper, the control scheme in Fig. 22 will be referred to as "Current Control" Grid ForMing, CC-GFM in short.

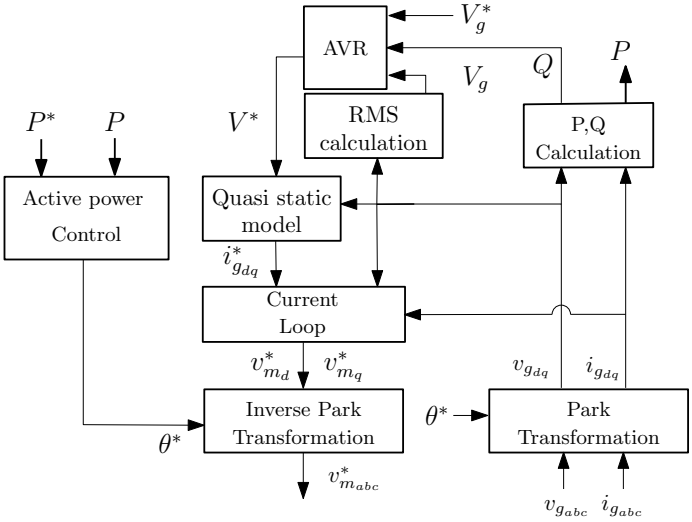

Fig. 22: Overall structure of grid forming control with current control loop

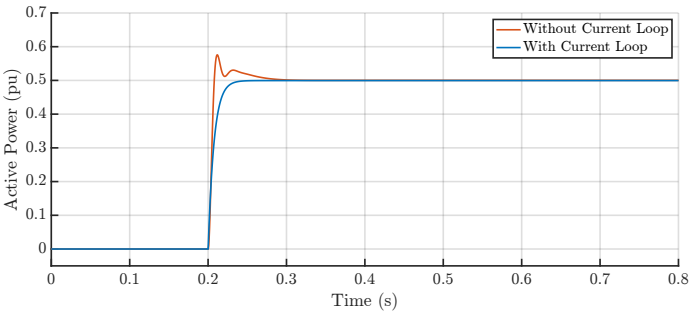

Fig. 23: Simulation of open-loop active power control with a current control loop

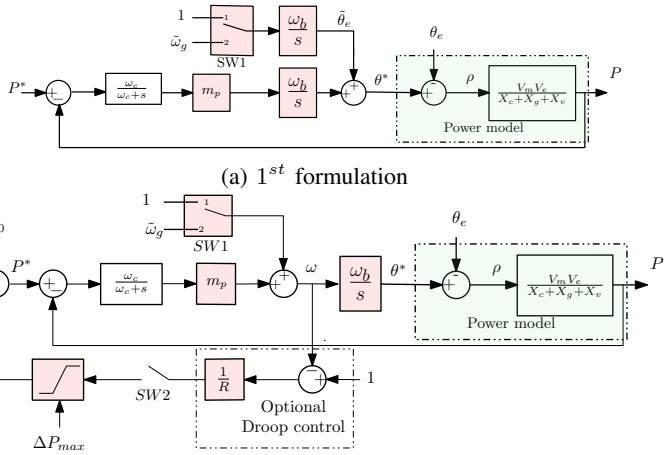

(a) 1^{st} formulation

(b) 2^{nd} formulation

Fig. 24: Closed-loop active power control

D. Closed-loop active power control

We now get to the point of devising a closed-loop active power control. Since the static model in Fig. 20 has been shown to be a valid approximation of the system dynamics, it can be used to design the sought controller. A step-by-step approach is followed hereafter to define the various types of control applied when opting either for VC-GFM or for CC-GFM. The type of controller depends on the requirements for the closed loop system.

The starting point is the very simple active power controller presented in Fig. 24a. In this scheme, the voltage angle θ_e can be seen as a disturbance for the active power control. The corresponding estimate $\tilde{\theta}_e$ acts as a feed-forward action. It is calculated by integration of the nominal voltage (SW1 in position 1). Hence, a simple integral action is enough to obtain an accurate control of the power. Generally, a first-order filter $\frac{\omega_c}{\omega_c+s}$ is included to avoid the double-frequency oscillations of power in case of unbalanced operation.

A simple reorganisation of that scheme yields the one shown in Fig. 24b. Considering for the time being that the switch SW1 is on position 1 and, SW2 is open, this control corresponds to the so-called “droop control”. The name comes from the variation of the active power proportionally to the frequency deviation. Indeed, in steady state, the voltage frequency ω, is equal to the grid frequency ω_g. Hence, assuming that the upper selector is in position 1, it can be written:

$$\omega_g = \omega = 1 + m_p \left(P^* - P\right) \tag{24}$$

or equivalently:

$$P = P^* + \frac{1}{m_p}\left(1 - \omega_g\right) \tag{25}$$

which is a classical frequency control equation with m_p as the droop coefficient. This can be seen akin an ”embedded” primary frequency support. However, it is not possible to limit the contribution of the VSC to this primary frequency support.

If the VSC is not intended to participate in frequency control, it is possible to cancel its contribution by using the estimate $\tilde{\omega_g}$ of the grid frequency, i.e. (SW1 in position 2). In this case, Eq. (25) becomes:

$$P = P^* + \frac{1}{m_p}\left(\tilde{\omega_g} - \omega_g\right) \tag{26}$$

Since $\tilde{\omega_g} = \omega_g$ in steady state, it can be deduced that the active power P is equal to its reference P^*. In the case of a fast frequency estimation, the embedded frequency support contribution mentionned above can be considered as cancelled.

Then, it is possible to add an external frequency droop control of the type used in speed governors synchronous machines (see Fig. 24b with the SW2 closed). It is also possible to limit the contribution to frequency support to a predefined value ΔP_{max}.

Another solution consists of adding an integrator in the loop as shown in Fig. 25a. Indeed, in steady state, the input of the added integrator should be zero, the active power P is then equal to its reference P^*. In this second-order system, the parameters could be adjusted for proper placement of the two poles [115], [116].

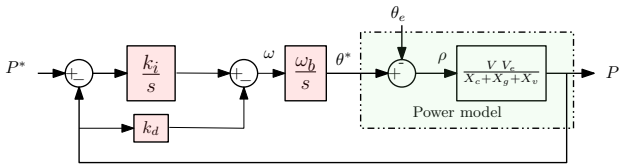

(a) Adding an integrator in the loop

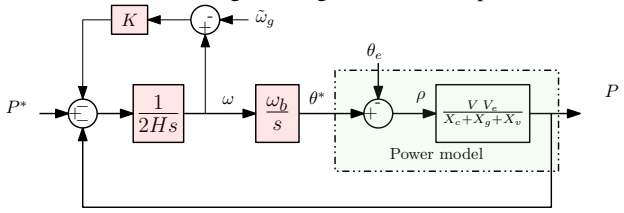

(b) VSM configuration

Fig. 25: Closed loop active power control with an inertial effect

It is possible to use the added integrator to emulate an "inertial" effect. Consider provisionally that $k_d = 0$. The following equation can be easily derived from Fig. 25a:

$$P = P^* - \frac{1}{k_i} s\,\omega \tag{27}$$

which reminds the link between the active power and the derivative of frequency (classical "swing equation") in a synchronous machine. Referring even more to the synchronous machine, the coefficient $1/k_i$ in Eq. (27) can be redefined as:

$$\frac{1}{k_i} = 2H \tag{28}$$

where H plays the role of the inertia coefficient (of the rotating masses) in a conventional power plant. Typically, the value of H will be chosen to meet system inertia (i.e. rate of change of frequency) requirements, while the choice of k_d remains a degree of freedom. It can be chosen to obtain a satisfactory dynamic response, as explained next.

Assuming $V_m \approx 1$ and $V_g \approx 1$, the transfer function between P and P^* can be obtained as:

$$\frac{P}{P^*} = \frac{1}{1 + 2Hk_d s + \frac{2H(X_c+X_g+X_v)}{\omega_b} s^2} \tag{29}$$

For this second-order system, the damping ratio ζ and the frequency ω_n are given by, respectively:

$$\zeta = k_d \sqrt{\frac{H\omega_b}{2(X_c + X_g + X_v)}} \tag{30}$$

$$\omega_n = \sqrt{\frac{\omega_b}{2H(X_c + X_g + X_v)}} \tag{31}$$

With the already mentioned single degree of freedom it is not possible to control both ω_n and ζ. A natural choice consists of specifying the damping. For a desired value $\tilde{\zeta}$, the corresponding value of k_d can be obtained by inverting Eq. (30):

$$k_d = \tilde{\zeta} \sqrt{\frac{2(X_c + X_g + X_v)}{H\omega_b}} \tag{32}$$

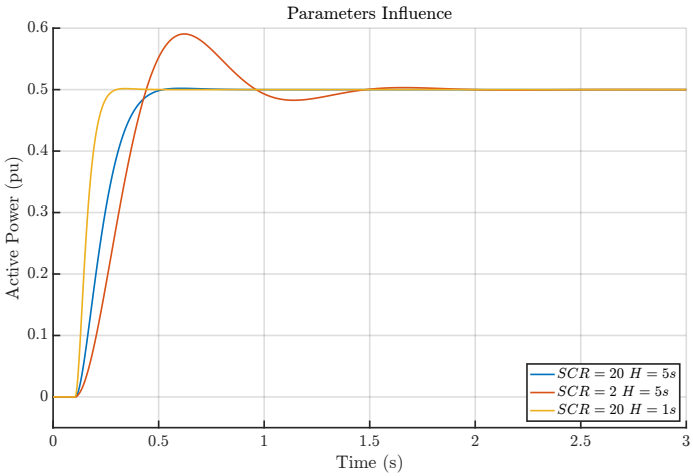

Fig. 26: Simulation results with a PI controller – 0.5 step on the active power reference

TABLE I: List of parameters for the control

Type of control	Parameter	Value
	H	5 s
	ζ	1
	X_v	0.3
VC-GFM	R_v	0.09
CC-GFM	ω_v	100 rad/s
	current loop dynamic	3000 rad/s

This equation highlights that an estimate of the grid reactance X_g is needed to determine k_d. In the absence of any information, a zero value can be assumed for X_g, which means that k_d is adjusted for a strong grid. As (31) highlights, ω_n depend on the value of H as it has been showcased in Section V-A.

A well-known alternative is the Virtual Synchronous Machine (VSM) scheme shown in Fig. 25b. The similarity of this scheme with the one in Fig. 25a has been shown in [101]. The first can be modified to yield the second, and conversely. In particular, the same damping is obtained by setting:

$$K = \frac{2Hk_d\omega_b}{X_c} \tag{33}$$

in the VSM scheme.

Fig. 26 a shows the simulation results for a PI controller in case of a strong grid (SCR = 20) when the value of $\tilde{\zeta}$ is set to 1. The general behaviour is similar to a second order system with a 5% overshoot as expected. The simulations have been done for VC-GFM and CC-GFM, the results are superimposed so only one result has been shown in this figure. When the SCR decreases to 2, the value of the grid reactance increases, then the damping ratio is decreasing as shown with (30). Many more simulation results can be found in [117]. The table below is a summary of the control parameters which will be used on the following sections.

E. Current saturation and Large Disturbance Stability

As it is well-known, the power electronic converters cannot handle large currents like synchronous machines. Consequently, in case of a large disturbance, a current limitation

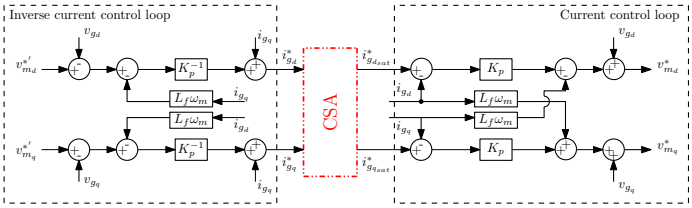

Fig. 27: Artificial threshold current loop and its inverse structure.

must be included in the control system to protect the converter. When this disturbance is ended, the question of resynchronization has to be studied carefully in order to recover a stable post-fault operation. These are the two aims of this section.

1) Solutions for Current Limitations in Grid-Forming Control: In order to limit the current, the virtual reactance-based method stands out as a well-known approach for current limitations in the literature [118], [119]. The basic idea is to increase the virtual reactance already presented earlier in this article. This transient reactance value is dynamically adjusted with respect to current limitation criteria, activated when the current exceeds a specific threshold I_n. A possible solution is described by the following equations:

$$X_{VI} = \begin{cases} K_{p_{P_{VI}}} \sigma_{X/R} \delta I \ if \ \delta I > 0 \\ 0 \ if \ \delta I > 0 \leq 0 \end{cases} \tag{34}$$

$$R_{VI} = X_{VI} / \sigma_{X/R} \tag{35}$$

Where $\delta_I = I_g - I_n$. $K_{p_{P_{VI}}}$ and $\sigma_{X/R}$ denote the virtual reactance proportional gain and virtual reactance ratio, respectively. For further insights into the optimal parameter selection, additional details can be found in [120].

Another method is called the Current Saturation Algorithm (CSA). It entails a current control responsible for determining the saturated current [121], [122]. To limit the current, the current references have to be saturated. In the case of a CC-GFM, the current loop is already implemented and the CSA can be reduced to a limitation of current references. In the case of a VC-GFM, current control is artificially introduced and canceled out by ‘”inverse current control” [122]. Fig. 27 presents a simple example with a proportional controller, but it can be extended to other types of controllers. In normal operation, the initial voltage references remain unchanged ($v^*_{m_d} = v^{*'}_{m_d}$). However, when a current limitation is needed, the ”CSA” block saturates the current references.

2) Impact of Current Limitation Type on Large Disturbance Stability: While the current has been limited, the question of restoring a stable operating point when the disturbance is canceled needs to be addressed. The classical $P(\delta)$ curve can be employed, similar to its application in transient stability analysis of synchronous machines. The extended $P(\delta)$ equation including the additional virtual reactance X_{VI} is given in the following equation:

$$P_{VI}(\delta) = \frac{VV_e}{X_c + X_g + X_v + X_{VI}} \sin \delta \tag{36}$$

In normal operation, $X_{VI} = 0$. However, in the case of a current limitation, $X_{VI} \neq 0$ due to the use of the virtual reactance method. Consequently, the maximum value of $P(\delta)$ decreases. In this context, Fig. 28 illustrates a scenario that may arise in the case of a bolted fault. Under normal operating conditions, $P(\delta)$ intersects with the power reference P^* at the point 1. When the fault is applied, P decreases rapidly till point 2. At this stage, δ increases while P remains at a very low level. At point 3, the fault is cleared, leading to an increase in active power; however, the current limitation remains activated. In the case of using a virtual reactance, the active power increases until the curve $P_{VI}(\delta)$ is reached (point 4). It will be shown in the dynamic simulation that the angle decreases when the active power P is superior to P^*. Due to the higher damping coefficient of a grid forming compared to a synchronous machine, there is nearly no overshoot on the angle when the fault is cleared. Hence, the Equal Area Criterion cannot be applied to the grid-forming control. After reaching point 4, the angle decreases until it reaches the original $P(\delta)$ at point 5 and then converges to the original operating.

In case of using the CSA method, the $P_{CSA}(\delta)$ is given by the following equation [123]:

$$P_{CSA} = \frac{VV_e I_{max}}{\sqrt{V_m^2 + E_g^2 - 2E_g V_m \cos \delta}} \sin \delta \tag{37}$$

The operation could be the same, but the angle at the fault clearance was such that the active power P is lower than P^* after the fault. Consequently, the angle continues to increase and the system is unstable. The limit stability angles ($\psi_{max_{CSA}}$, $\psi_{max_{VI}}$) are illustrated for both current limitation methods. It can be deduced that this classical CSA method provides less stability margin than the virtual reactance approach. Further insights provided in [110], [124] underscore the coupling of current saturation with active power control, resulting in a reduction in the critical clearing time. Indeed, Eq. (37) illustrates how active power expression varies with the current saturation state, influencing the system's stability limit.

This analysis is based on a static model; however, it is essential to validate the model's accuracy through dynamic simulations.

Accordingly, an 80% voltage drop is applied to a Thevenin equivalent voltage source during 200 ms. The VC-GFM of Fig. 27 is implemented with $H = 5s$ and a 0.3 pu virtual reactance. The initial state of active power is set to 0.8 pu.

Fig. 29a confirms the general trends given by the static model. Although some dynamic phenomena are noticed, the operating points observed are in line with those given by the static model and the system remains stable after the fault clearance. Fig. 29b showcases the evolution of the main electrical variables with respect to the time. It has been checked with dynamic simulation that in the case of employing CSA, the system becomes unstable.

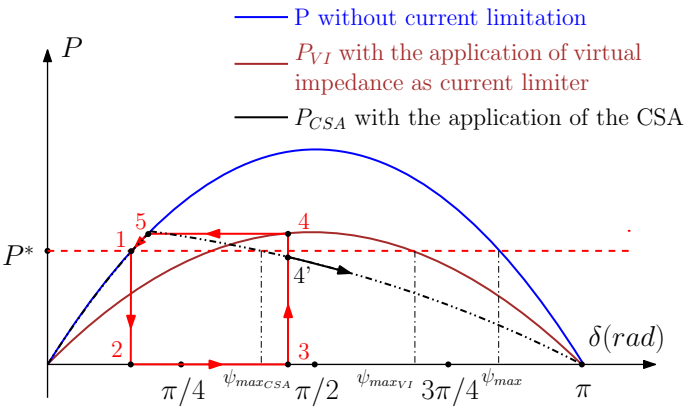

Fig. 28: Schematic representation of $P(\delta)$ under normal conditions and during current limitation.

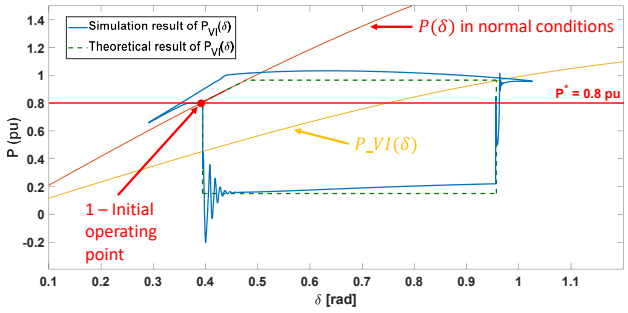

(a) Power angle curve

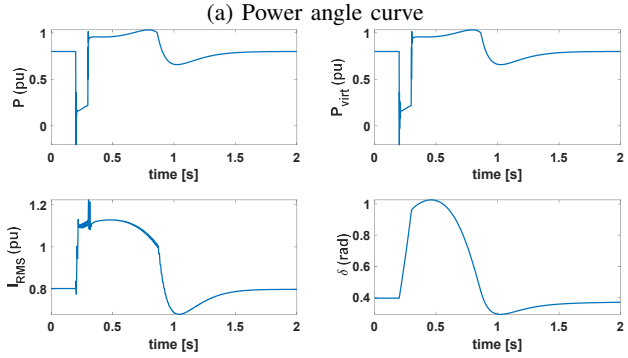

(b) Dynamic response

Fig. 29: System response to 200 ms grid fault during the application of the current limitation.

3) Improving Large Disturbance Stability through the Virtual Power Method: Numerous approaches have been published to increase the stability margin of GFM control during large stability disturbances. One approach involved using a PLL during current saturation and refining synchronization angle control [125], [126]. However, this method requires a complex control structure and a thorough understanding of PLL-related dynamics.

Additionally, recent research [127] proposes enhancing large disturbance stability through modifications to voltage reference control. It aims to improve the angle stability of large signals by modifying the acceleration and deceleration zones. Indeed, it leads to an increase in the maximum of the characteristic $P(\delta)$, particularly during the fault. However, it is noteworthy that the new characteristic obtained remains lower than the blue curve of Fig. 28 during the fault. Consequently, the new characteristic may also be below the P^* for a severe grid fault then leading to instability.

A method referred to as "virtual power" was introduced for the CC-GFM in [123] in order to enhance the large disturbance stability. The original version of the virtual power method is based on the CC-GFM control. It uses the unsaturated current output from the quasi-static model (see Fig. 31) to generate the virtual power P_{virt}:

$$P_{virt} = v_{g_d} i^*_{g_d} + v_{g_q} i^*_{g_q} \tag{38}$$

In Fig. 31, $i^*_{g_{dqsat}}$ represents the saturated currents used as references for the current loop. They are derived from the unsaturated references $i^*_{g_{dq}}$, divided by a proportional coefficient K such that:

$$i^*_{g_{dq_{sat}}} = i^*_{g_{dq}}/K \tag{39}$$

Applying Kirchhoff's equations between PCC and the grid voltage source yields:

$$v_{g_{dq}} = v_{e_{dq}} + jX_g i_{g_{dq}} \tag{40}$$

Merging these two equations, (22) and (23), leads to the virtual system equation:

$$V^* = v_{e_d} + (X_c + X_v + X_g/K) i^*_{g_q} \tag{41}$$

$$0 = v_{e_q} - (X_c + X_v + X_g/K) i^*_{g_d} \tag{42}$$

It results in the following expression for the virtual power $P_{virt}(\delta)$ curve:

$$P_{virt} = \frac{VV_e}{X_c + X_v + X_g/K} \sin\delta \tag{43}$$

During normal operation $P_{virt}(\delta)$ is similar to $P(\delta)$ since $K = 1$. In case of current limitation K becomes larger than 1, then the maximum of $P_{virt}(\delta)$ is greater than the maximum of $P(\delta)$. The most interesting feature of this method that, with the use of the virtual power, the virtual operating point can seamlessly converges towards this curve in case of large disturbance without any apprehension of over-current in the real current, as this latter is effectively limited by the CSA. Since this $P_{virt}(\delta)$ has been enlarged compared with the two previous methods, the large disturbance stability is improved for the virtual power and also for the real system since it is closely linked to the virtual one. In other words, it can be seen that there is a decoupling between the large disturbance stability enhancement principle and the current limitation.

Fig. 30 illustrates the theoretical evolution of the virtual power following a bolted fault. The same types of operations can be observed as those explained in the previous section, except that the $P_{virt}(\delta)$ has been enlarged, making it more likely that the virtual system will recover its initial operating point after the transient.

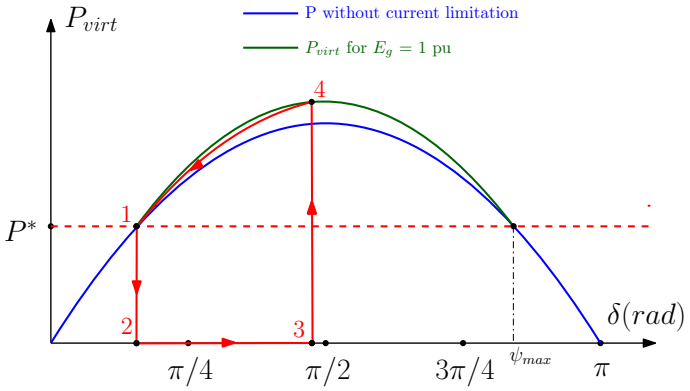

Fig. 30: Schematic representation of $P(\delta)$ with the implementation of the virtual power.

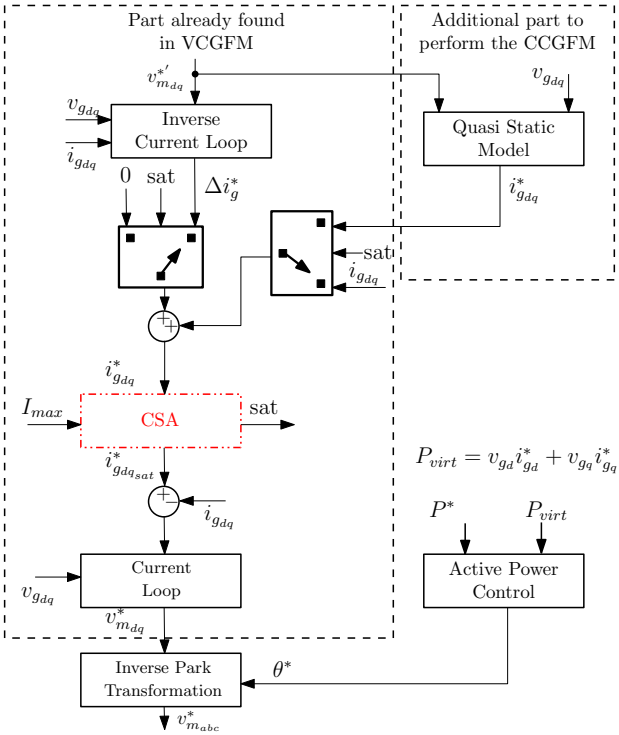

Fig. 31: Presentation of VC-GFM architecture with the implementation of the virtual power method.

4) Application of Virtual Power Method to VC-GFM: Expanding upon the proven efficacy of the CC-GFM architecture in handling large disturbance stability, it is proposed to adapt the virtual power method for the VC-GFM.

The key idea is to apply the principle of the inversion control loop to maintain the VC-GFM control scheme in normal operation, and to switch to CC-GFM in the case of current saturation, as shown in Fig. 31. Subsequently, the virtual power method, as previously described, can be applied during large disturbances.

To assess the effectiveness of the proposed method, a 200 ms bolted fault is applied to the equivalent Thevenin voltage source of the grid. Furthermore, the SCR is decreased

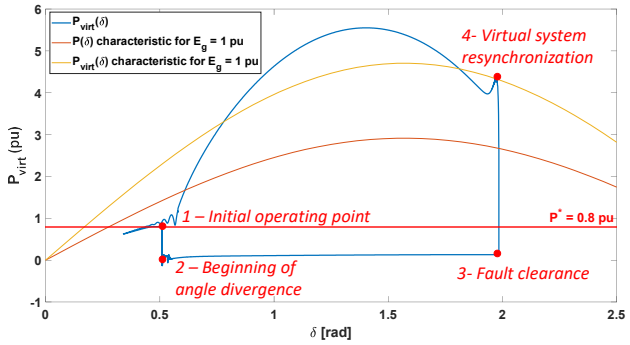

Fig. 32: System response of the system following a 200 ms grid fault.

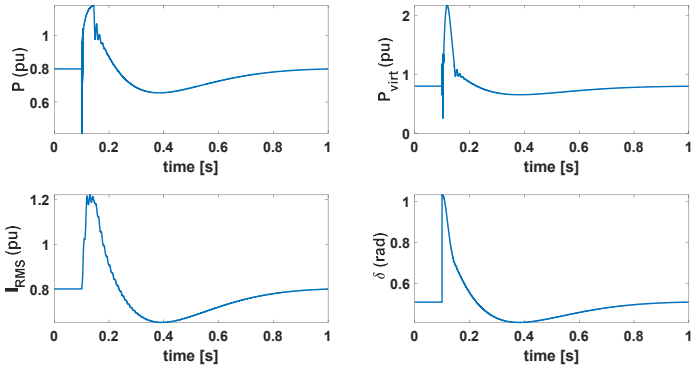

Fig. 33: Dynamic response of the system following a $-\pi/6$ phase shift.

to 5. The initial state of the system is the same for the case of Fig. 29. Even if the virtual power is not following exactly the theoretical curve, the dynamic evolution noticed in Fig. 32 is in line with the anticipated behavior described in Fig. 30. This similarity enables the system to restore synchronization following a bolted fault occurrence.

Furthermore, an enhancement to the virtual power method has been proposed, as detailed in [128]. This modification aims to improve system dynamics and accelerates the restoration process following fault clearance.

To further evaluate the virtual method within the hybrid architecture depicted in Fig. 31, a phase shift of $-\pi/6$ is implemented. As illustrated in Fig. 33, the system restores synchronization effectively as observed in a bolted fault scenario.

F. Stabilizing effect of the grid forming control

While there is a consensus that GFM controls are expected to provide services to the grid to counter the destabilizing impact brought by the decrease of synchronous generation and the increase of conventionally controlled PEIR, their study has been mostly limited to their own stability in weak grids and their provision of inertia and frequency control [129]. This section is focused on the small signal stabilizing effect provided by a GFM converter applied to a small benchmark.

As shown earlier in subsection VI-D, the GFM active power control can follow different schemes with a similar level of

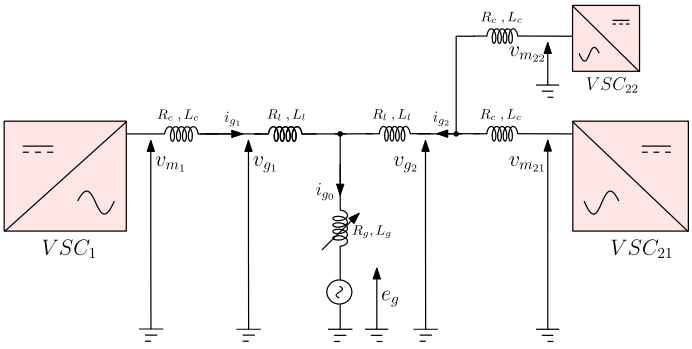

Fig. 34: Description of the test setup with a passive load

TABLE II: Test setup parameters

Circuit	Parameter	Value
VSC	S_{nom}, S_b	1.044 GVA
	U_{nom}, U_b	400 kV
	P_{nom}	1 GW
	Q_{max}	300 MVAr
Filter	L_c	0.15 pu
	R_c	0.005 pu
OHL	L_l	0.144 pu
	R_l	0.0072 pu
Grid	L_g	1 pu
	R_g	0.1 pu

dynamic performance. Moreover, it has been demonstrated in subsubsection VI-E4 that a VC-GFM control can perform just as well as its CC-GFM counterpart during faults. Therefore, the question to ask is: for an identical active power control, does the presence of a current loop play a role in the stabilizing performance of GFM controls? This is investigated in the following.

1) A suitable test setup for small signal studies: Similarly to the previous sections, control studies are often based on a single converter connected to a Thévenin equivalent, also referred to as a Single Unit Infinite Bus (SUIB) setup. Most literature studies restrain the study of converter controls to this setup to assess their dynamic performance and conclude on their stability in weak grids. Small signal stability studies utilize this setup to provide tuning recommendations [130], [131], to assess controls stability limits, and to highlight the differences between different controls, such as GFM and GFL [132].

However, it has been shown that, for a properly tuned control, a Thévenin equivalent setup is not sufficient for small signal studies as it is limited by reactive power constraints rather than the dynamic performance of the controls [133]. Furthermore, the use of a SUIB cannot highlight any interaction phenomena among PEIR, which is an important phenomenon that needs to be accounted for [129]. While studies considering bigger systems can be found in literature, they have been limited to study cases with identical converters controls [134]. When both GFM and GFL converters are considered, the studies are either tuning oriented [135], [136], or assume that a GFM is equivalent to an infinite bus, thus regressing to a study with identical controls in the system [137]. When the stabilizing impact of GFM controls is directly targeted by a study [138], different GFM controls are considered as equally stabilizing, assuming adequate tuning and the study is based exclusively on time-domain simulations without any further insights on how GFM controls enhance the grid strength. A recent study has tackled this same question [139], but the controls did not account for the presence of a virtual reactance, which has been introduced in subsections V-D and VI-B

In this subsection, the setup proposed in [133] and enhanced in [139] is adopted and its state space model is analyzed. This setup is retained as it is unimpeded by the constraints of the SUIB setup, and yet simple enough for a comprehensive analysis of interaction phenomena behind the instability mechanisms. As shown in Fig. 34, the setup consists of three converters, where VSC_1 and VSC_{21} are controlled using a generic GFL control, as used in [139], and VSC_{22} is GFM-controlled using the IP scheme in Fig. 25a, with and without current control shown in Fig. 22 and Fig. 18. The converters are set up such as VSC_1 is the same size as the total size of VSC_{21} and VSC_{22}:

$$S_{nom}^{VSC21} + S_{nom}^{VSC22} = S_{nom}^{VSC1} = S_b \tag{44}$$

Where S_{nom}^{x} refers to the nominal power of x and S_b refers to the base power used for the per-unit. The parameters of the setup are detailed in Table II, where the per-unit values of the Overhead Lines (OHL) and the grid are based on S_b and U_b, while each converter filter per-unit (pu) values refer to the MVA base (S_{nom}^{VSC1}, S_{nom}^{VSC21} or S_{nom}^{VSC22}) of each converter. The operating point studied in this section is such that no power flows to the external grid, hence allowing the increase of the electrical distance to the infinite source without any static constraints, while the converters are at their nominal powers:

$$\begin{cases} P_{VSC1}^{*} = -(P_{VSC21}^{*} + P_{VSC22}^{*}) = -P_{nom} \\ V_{VSC1}^{*} = V_{VSC21}^{*} = V_{VSC22}^{*} = 1\ pu \end{cases} \tag{45}$$

Where $P_{VSC_i}^{*}$ and $V_{VSC_i}^{*}$ are the active power and voltage set points of each converter $i \in \{1, 12, 22\}$, respectively.

The setup at this operating point is representative of a study case of a remote transmission corridor, where VSC_1 is one end of an HVDC link evacuating the power generated by a wind farm split into a subset of generators in GFL mode (VSC_{21}) and another subset of generators in GFM mode (VSC_{22}).

2) Impact of GFM controls on the stability of the system: One way to highlight the stabilizing impact of the different GFM controls is by investigating the minimal size of the GFM-controlled VSC_{22} to reach the small signal stability of the system. As previously reported in [139], the VC-GFM control provides a stronger stabilizing effect compared to the CC-GFM alternative as a much smaller VC-GFM-controlled VSC_{22} is required to stabilize the setup. This observed difference can be reduced when considering passive loads but remains significant. Here, the same investigation is conducted to verify

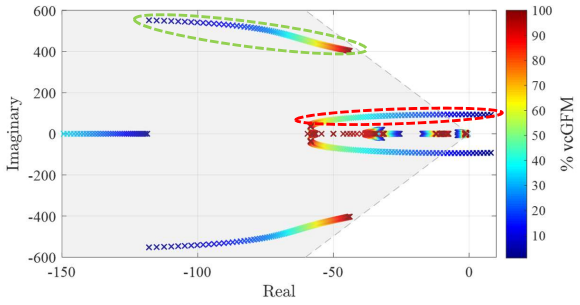

(a)

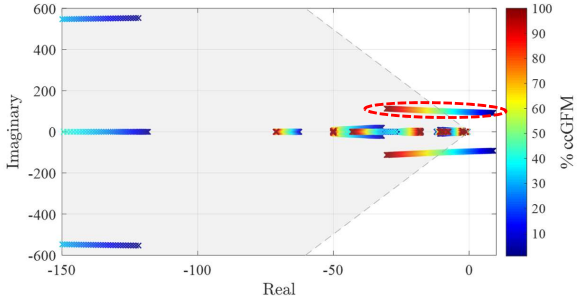

(b)

Fig. 35: System eigenvalues for varying VSC_{22} proportions under VC-GFM (a) and CC-GFM (b)

whether these trends stand when considering more complete GFM controls, including the virtual reactance and the AVR outer loop. In the same manner as [139], the state-space model of the full system is constructed, linearized, validated against EMT time-domain simulation and then analyzed. The grid reactance Z_g is chosen to reflect a weak grid, such as a 100% GFL system would be unstable, here: $Z_g = 1\ pu$. Using the linearized state-space model, a parametric sensitivity study is conducted to assess the minimal size, expressed in % of S_{nom}^{VSC22} relatively to S_b, of the GFM-controlled converter required to reach small signal stability. The results are illustrated in Fig. 35. It can be seen that only a 8% of VC-GFM control is sufficient for the system to regain small signal stability where 22% of CC-GFM would be needed. If an accepted dynamic performance is set as a damping ratio above 10%, the VC-GFM control complies with such a performance requirement for as little as 13% while the CC-GFM-controlled converter can only reach such a performance for a proportion above 53%.

It is worth noting that this gap widens if weaker grids are considered. For instance, for $Z_g = 2\ pu$, the minimum size of the GFM-controlled VSC_{22} is four times bigger if it's controlled under CC-GFM (84%) rather than VC-GFM (21%).

Such findings join the previous conclusions found in [139]: the VC-GFM control allows for stability and acceptable dynamic performance with a much smaller volume than its CC-GFM alternative.

Further studies using the participation factors of the dominant modes, encircled in Fig. 35, have allowed the confirmation of previous findings as well: the VC-GFM-controlled converter decouples the GFL-controlled converter from the weak grid, whereas the CC-GFM-controlled converter presents additional interactions due to its vulnerability to the PCC voltage (used for the QSEM).

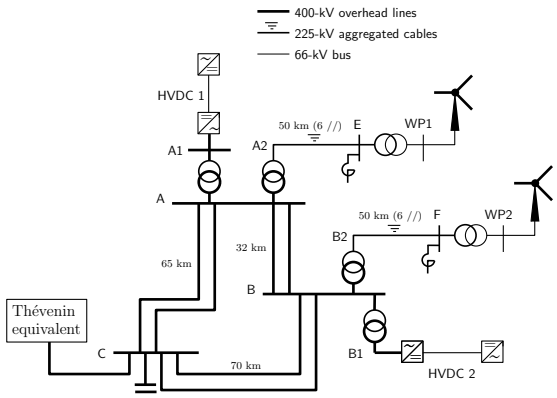

Fig. 36: The Four-VSC benchmark system

G. Extension of findings to a 4 VSC meshed benchmark

1) Introduction of the four-VSC benchmark system: A four-VSC benchmark system is proposed in this section to extend the previous findings. It has been designed to offer the following features:

- small enough for its stability margins to be easily assessed
- involving several VSCs electrically rather close to each other (to contemplate possible interactions)
- connected to an external grid of adjustable strength in terms of short-circuit power
- relying on generic models of the type used in the previous sections

The one-line diagram is shown in Fig. 36. The system hosts two wind parks (WP1 and WP2) and the terminal converters of two HVDC links (HVDC1 and HVDC2). The remote converter of each HVDC link is not modelled, the DC voltage being assumed constant. WP1 and WP2 are aggregated equivalents of a large number of generators. The connection transformers of all four VSCs are represented explicitly.

The connection to an external system is considered through the Thévenin equivalent attached to bus C. Since the Thévenin voltage source forces the system frequency to return to its nominal value in steady state, this 100% power-electronic converter based system is clearly not meant to address frequency issues.

The 400-kV part of the transmission grid is meshed, allowing to simulate the outage of one or two circuits without disconnection from the external system. The line lengths are given in Fig. 36. Each wind park is radially connected to the grid through six 225-kV cables and six transformers in parallel to cope with the maximum production of each park. The cables are 50 km long and correspond to the AC connection of an offshore wind farm. The shunt reactors at buses E and F aim

TABLE III: 4-VSC system: line and cable data

	R Ω/km	X Ω/km	$\omega C/2$ μS/km	S_{nom} MVA
400-kV*	0.016	0.320	1.5	1300
225-kV**	0.0084	0.017	180.0	2400

pertain to: * each circuit ** 6 cables in parallel

TABLE IV: 4-VSC system: transformer data

	R pu	X pu	n	S_{nom} MVA
A2 - A	0.005	0.15	1.02	2400
B2 - B	0.005	0.15	1.05	2400
A1 - A	0.005	0.15	1.02	1200
B1 - B	0.005	0.15	1.04	1700
WP1 - E	0.005	0.12	1.05	2400
WP2 - F	0.005	0.12	1.04	2400

at absorbing the excess reactive power produced by the cables. The line, cable, transformer and VSC parameters are given in Table III, IV and V, respectively.

The benchmark has been modelled and is studied in EMTP, where the 225kV cables were modelled using wideband cable models based on the physical and geometrical properties of the cables from [140].

By its meshed structure and the nominal power of its components, the present benchmark allows for the study of a large spectrum of operating points. For the following studies, two extreme operating points are retained and are detailed in Table VI.

H. Small signal stability properties of GFM controls

The purpose of the study is the verification of the varying stabilizing effects of the VC-GFM and CC-GFM controls. The chosen operating point is the first from Table VI, the wind parks inject the same power, most of which is evacuated by the HDVC links. This results in a lightly loaded network. At this operating point, the system stability is assessed in terms of minimal short-circuit power of the external system. The corresponding Thévenin reactance is varied. The net power injection of the VSCs (minus the network losses) is taken by the load at bus C, which results in no power flowing into the Thévenin equivalent. Hence, the initial state remains unchanged while the reactance is varied and there is no risk of reaching the (static) loadability limit of the equivalent (for large values of its reactance).

TABLE V: 4-VSC system: converter data

	S_{nom} MVA	P_{nom} MW
WP1	2400	2300
WP2	2400	2300
HVDC1	1200	1150
HVDC2	1700	1630

TABLE VI: 4-VSC system: operating points

operating point #	Power (MW) injected by WP1	WP2	HVDC1	HVDC2
1	1500	1500	-1120	-1600
2	1500	1500	1150	1400

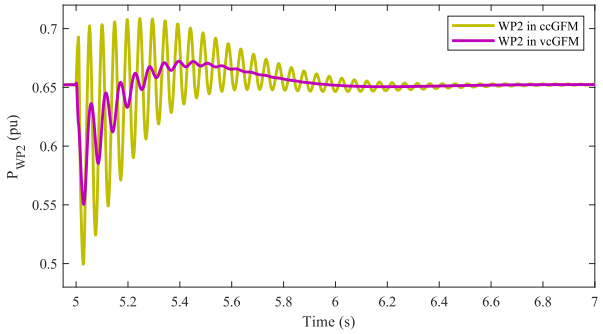

(a) Active power reaction to a small signal disturbance

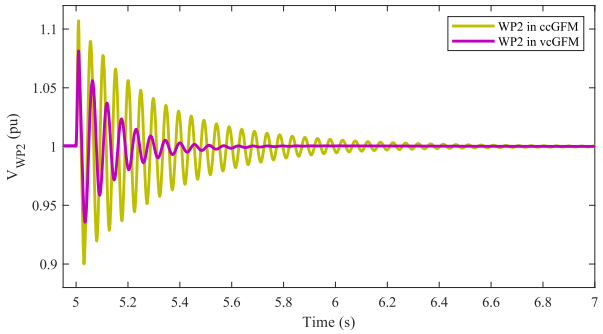

(b) Voltage reaction to a small signal disturbance

Fig. 37: WP2 reaction to a $\pi/40$ phase jump at the infinite voltage source

By setting the short circuit power provided by the external Thévenin equivalent at bus C to 8 GVA, the system is small signal-unstable if all converters are controlled in GFL mode. However, by controlling the second wind park (WP2) with a GFM mode, the system regains small signal stability as shown in Fig. 37a and Fig. 37b, where the power and voltage of WP2 are measured after the system experiences a $\pi/40$ phase jump at the Thévenin equivalent voltage source. Furthermore, it can be observed that when WP2 is VC-GFM-controlled, the system displays a better damping, more precisely double the damping ratio, than when it is CC-GFM-controlled. If the external grid is made even weaker, the study case with the CC-GFM controlled WP2 is the first to become small signal unstable, which goes to confirm the previous trends regarding the difference in stabilizing properties of VC-GFM and CC-GFM schemes.

1) Large Disturbance Stability: As confirmed by the previous section, the VC-GFM control provides a better stabilizing effect within the scope of small signal stability. The next verification to be made is whether this control is compliant with large disturbance requirements [141], [142]. Here, the second operating point of Table VI is considered, this results in a heavily loaded network, both wind parks and both HVDC links injecting active power into the grid. Nevertheless, the system is N-1 secure with respect to the outage of any 400-kV circuit. No load is present, hence, the whole production (minus the network losses) is exported to the external system

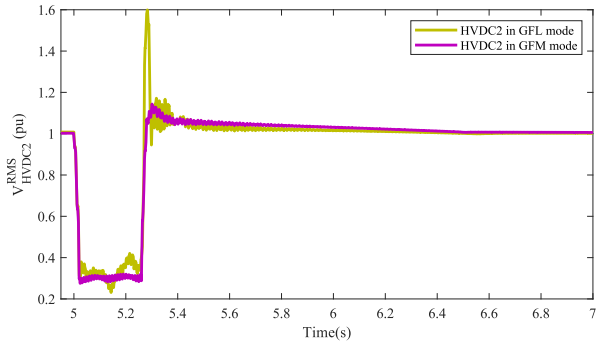

(a) HVDC2 Voltage reaction to a large signal disturbance

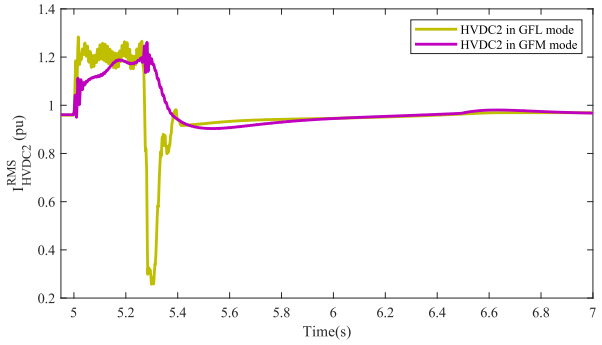

(b) HVDC2 injected current reaction to a large signal disturbance

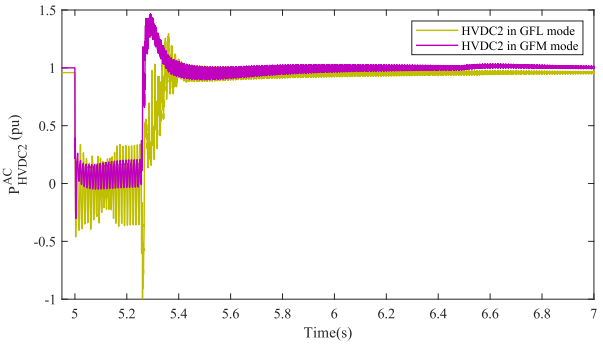

(c) HVDC2 active power reaction to a large signal disturbance

Fig. 38: HVDC2 reaction to a 200ms three-phase fault followed by a line trip

represented by the Thévenin equivalent at bus C. The short-circuit power is set higher than the previous case to allow the evacuation of the power injected by the HVDC links and wind farms, while the system is small signal stable even for when all converters are in GFL mode.

The most severe large disturbance event considered here is a 250 ms three phase fault at the most loaded line of the system, here one of the A-C lines transmitting 1.5 GW each, followed by the opening of this line.

Using this operating point and disturbance event, the controls large disturbance stability is tested. All converters are first in GFL mode, then HVDC2 is switched to VC-GFM mode. For the GFL converters, in addition to the structure shown in [139], a Fault Ride Through (FRT) block is added to the control to limit the currents in order to protect the converters, to dynamically support the voltage during the fault and to allow a slow active power recovery. The detailed control structure is available in [117]. For the VC-GFM converter, the control shown in Fig. 31 is used.

The EMT time domain simulations conducted in EMTP, presented in Fig. 38, show that currents are successfully limited in both cases. However, when all converters are in GFL mode, the post fault overvoltage is dangerously high and the system displays an oscillatory behavior post fault. On the other hand, when HVDC2 in VC-GFM mode, the currents smoothly transit from the saturated limit to their steady state value, with the active power response remaining within the TSOs required response time. Moreover, the post fault overvoltage is significantly reduced and the oscillations are better damped.

This study case shows that even under the most demanding large disturbance event, the solution identified as best for small signal stability (here, VC-GFM) succeeds at complying with large disturbance stability requirements in a more realistic system than a SUIB setup.

VII. Conclusion

The promises and challenges of GFM solutions have been discussed, starting with an overview of the system needs and the corresponding requirements applied by various TSOs to grid-connected assets, notably PEIR. Subsequently, we delved into the development of cost-effective technical solutions from the perspectives of a BESS developer and a manufacturer of HVDC systems. Finally, we presented the academic viewpoint on GFM models and control strategies. Key takeaways from the TSOs and BESS developer can be enumerated as follows:

1) Power system security relies on a volatile balance between the varied immunity of grid-connected devices and the overall system performance. As power system dynamics evolve, this equilibrium shifts. The greater the sensitivity of grid users, the more demanding the requirements on TSOs to constrain electrical quantities under plausible contingencies, and vice versa. Therefore, both withstand capabilities and performance requirements are systematically addressed through CNC.
2) By contributing to system strength, inertia, and damping, GFM resources serve as pillars for the stable operation of power systems, alleviating constraints on other grid users. *The more, the merrier* premise applies; as the requirement extends to a greater number of devices, constraints are expected to decrease for all grid users.
3) Similar to SG, PEIR can, to some extent, contribute to system stability as a by-product of their main purpose to limit the deployment of dedicated assets. However, this behaviour is not inherent; it must be specified.
4) Depending on the specific formulation of a new requirement applied to a given facility, it may entail either minimal design modifications (limited to control updates) or hardware upgrades. Consequently, the description of the GFM capability has evolved with industry understanding of the burden it may pose on equipment sizing.

5) GFM capability is an addition to existing resource-specific technical requirements. In some cases, updates may be needed for ensuring compatibility among them.
6) GFM *Core* requirements, applied *within current and inherent energy limits*, have demonstrated no significant impact on installation design. However, the addition of advanced features, such as high FFCI, harmonic filtering, or black start capability, essential for secure operation in specific conditions, may involve oversizing power elements or changes in operational practices. Therefore, their deployment necessitates detailed cost-benefit analyses. Pilot projects for both use cases exist.
7) For resources with low to no inherent energy storage, the inertial response may fall into the *additional* requirements category. In operation, procedures to reserve headroom capacity may be required to ensure availability.
8) GFM BESS can provide SCL and Inertia in effective way by optimizing the plant design to the system needs. In addition, by stacking multiple revenue streams on top of stability services, BESS can provide greater overall benefits to both SO and consumers by being able to provide all these services in parallel at lower cost.
9) Challenges in exploring the deployment of GFM on PEIR are partially due to the variety of control solutions in the literature. Many rely on using active power measurement for synchronisation instead of estimating the voltage phase at the unit's terminal and consider specific current limitation strategies.
10) In practice, various solutions may provide similar functionalities and performances. Within a predefined validity domain, their contribution to system stability can be evaluated using simplified generic models. This is particularly relevant for TSOs when project-specific models are unavailable, as usually during the planning stage.
11) For system design and interaction studies, typically during compliance verification for grid connection, detailed EMT vendor models are necessary. This is true in general not only for studies involving GFM. FAT based on HIL platforms are also valuable tools.

Although the GFM denomination originally referred to a type a control, it has now been adopted by TSOs to designate a specific set of features, performance-based requirements, to guide OEM in the product development. Regarding the challenges that lie ahead, widespread KPI characterizing the decreasing voltage stiffness, and thereby, increasing instability risks, include system (or regional) inertia and *system strength*. To inform decision-making at both planning and operational stages, additional efforts are required on their quantification and monitoring to account for PEIR. Suitable operational procedures and mitigation measures should also be developed.

In the manufacturer part of the paper, it has been illustrated how different requirements are reflected on converter performance. Some emphasis has been put on the internal DC side behaviour of the converter, which is often overlooked. The impact on converter and AC system performance of large system disturbances in combination with virtual inertia and virtual reactance has been illustrated through simulations. The possible contradictions between inertia requirements and desired response speed of the control have also been stressed. A general conclusion is that it is important to keep the disturbance specifications at a realistic level to avoid oversizing the converter and, hence, unnecessary costs. In the same way, the transmission and current capability of the converter should be respected in order to guarantee performance. In a severe case, the converter may even trip jeopardizing stability of the system. The converter dimensioning may then need to be increased, which in turn will increase the cost. To give an example, a large phase jump may be the dimensioning scenario for the converter design. As long as general HVDC performance is of concern, generic models and control system representations make up a valuable basis of discussions regarding control impact on system performance between TSOs and manufacturers. For detailed design studies, a manufacturer model with a detailed representation of the DC side and accurate time delays will always be needed.

As it has been shown in the TSOs section, the classical GFL converters are not aligned with the system needs: it is required to equip the grid with some voltage sources. However, the description of a grid forming VSC as a "voltage behind and reactance" is not sufficient: it has to be coupled with a compulsory active power control of the converter. Combining both properties leads to the concept of power synchronisation control, which is the basis of grid forming control.

In the academic section, a consistent methodology has been proposed to design this control. In a first step, the validity of approximating the dynamic model by a much simpler static model has been established whether a current loop is present or not. In a second step, this single model enabled a unified approach for the design of the active power loop. By using this model, two types of control have been derived depending on the requirement for an inertial effect or not. All the parameters of the control have been justified. In particular, the motivation of using the estimate of the grid frequency in the droop control scheme has been stressed, in order to decouple the active power loop dynamics from the primary frequency control with droop.

The corresponding models have been tested for various events on a Thévenin equivalent to check the dynamic behaviour of the system either in normal operation or in case of current limitation. Unlike the synchronous machine, the controls of a grid forming converter make it possible to manipulate the voltage angle to significantly stabilize its response to short-circuits or phase shifts. Incidentally, this discourages using the term "virtual synchronous machine" in so far as the dynamic behaviour of the grid forming converter with inertial effect is very far from that of a synchronous machine. Furthermore, using the virtual power method allows decoupling the current limitation from the large-disturbance stability enhancement.

In order to study interactions between converters, a dedicated benchmark has been proposed. It allows studying the dynamics of the system is case of very weak grid without hitting

the static loadability limit of a Thévenin equivalent. The significant difference in terms of stabilizing effect of respectively the VC-GFM and the CC-GFM have been highlighted. Next, a four-VSC benchmark system has been proposed to increase the complexity of the system under study. This benchmark opens the way to a wider range of tests and already confirms the findings drawn from the previous tests. The benchmark is fully documented and its model its parameters are available in open source [ref]. It is hoped that the models and data in this benchmark will serve as reference when proposing alternative control schemes, but also when validating them on commonly shared test cases and scenarios, which is seldom the case in the available literature.

To summarize, this part of the paper has proposed a generic and coherent approach to grid forming control; it is hoped to provide underlying concepts leading to better understanding of this promising technology (and, hopefully material for teaching this topic !). The proposed models are well in line with TSO requirements in terms of bringing stability, strength and inertia to the grid.

Of course, not all aspects of grid forming have been addressed in this paper. For instance this work has been successfully extended to more realistic converters such as MMC [143]. It appears that, in normal operation, the behaviour of this converter is very similar to an ideal VSC. In case of large disturbance, it may be needed to adjust some low level controls to achieve a good balance of the energy in the hundreds of submodules. Some extensions of the methodology outlined in this paper to medium-voltage VSCs have been also considered [96]. This requires to control the internal energy of the LC filter and to take into account the non negligible resistive component of the grid.

The last words will be to quote a few directions for future work:

1) The integration of the negative sequence in the GFM control: the two types of control, with and without current loop, can be applied to the treatment of the negative and positive sequence. This includes the definition of optimal references for the positive and negative current/voltages.
2) Some works have already been successfully performed [144], [145] to extend the concept of using the voltage angle to control the DC bus voltage of an HVDC link. This is a kind of extension of the power synchronisation control concept. The first results clearly highlight that this type of control is also bringing stability to the system.
3) Once the model is well defined, it is possible to enlarge the analysis to system-wide (large-scale) studies such as optimal placement of the GFM converters or studies involving converter-driven instability of the slow type [146] and possibly interactions with other stability issues, such as short-term voltage instability.

DISCLAIMER

The views expressed in this article are those of the authors and not necessarily those of AEMO. The information in this article does not constitute technical, legal or business advice. Before relying on it, you should make your own enquiries.

REFERENCES

[1] Migrate H2020, "D3.1 description of system needs and test cases," 2016. [Online]. Available: https://www.nationalgrideso.com/document/84261/download

[2] National Grid, "System needs and product strategy," 2017. [Online]. Available: https://www.nationalgrideso.com/document/84261/download

[3] J. Bialek, T. Bowen, T. Green, D. Lew, Y. Li, J. MacDowell, J. Matevosyan, N. Miller, M. O'Malley, and D. Ramasubramanian, "System needs and services for systems with high ibr penetratio," 2021.

[4] Energy System Integration Group, "Grid-forming technology in energy systems integration," 2022.

[5] "Great britain grid forming best practice guide," 2023. [Online]. Available: https://www.nationalgrideso.com/document/278491/download

[6] ACER, "Draft: Network code on requirements for grid connection of generators v2," 2023. [Online]. Available: https://www.acer.europa.eu/sites/default/files/documents/Recommendations_annex/ACER_Recommendation_03-2023_Annex_1a_NC_RfG_TC_to_original.pdf

[7] AEMO, "Voluntary specification for grid-forming inverters," 2023. [Online]. Available: https://aemo.com.au/-/media/files/initiatives/primary-frequency-response/2023/gfm-voluntary-spec.pdf

[8] RTE, "Bilan annuel de la qualité de l'électricité," 2022.

[9] Bureau of Meteorology, "Severe thunderstorm and tornado outbreak south australia 28 september 2016," 2016. [Online]. Available: http://www.bom.gov.au/announcements/sevwx/

[10] AEMO, "Black system south australia september 2016 report," 2017. [Online]. Available: https://www.aemo.com.au/-/media/files/electricity/nem/market_notices_and_events/power_system_incident_reports/2017/integrated-final-report-sa-black-system-28-september-2016.pdf

[11] ENTSOE, "Network code on requirements for grid connection of generators," 2016. [Online]. Available: http://data.europa.eu/eli/reg/2016/631/oj

[12] "Ieee standard for interconnection and interoperability of inverter-based resources (ibrs) interconnecting with associated transmission electric power systems," *IEEE Std 2800-2022*, pp. 1–180, 2022.

[13] "Nf en 50549-2:2019 requirements for generating plants to be connected in parallel with distribution networks - part 2: Connection to a mv distribution network - generating plants up to and including type b," 2019. [Online]. Available: https://standards.iteh.ai/catalog/standards/clc/bd975a08-a7fc-47a1-9e46-b9c96cc2dafe/en-50549-2-2019

[14] Z. H. Rather and D. Flynn, "Impact of voltage dip induced delayed active power recovery on wind integrated power systems," *Control Engineering Practice*, 2017.

[15] AEMO, "System strength requirements methodology," 2022. [Online]. Available: https://aemo.com.au/-/media/files/electricity/nem/security_and_reliability/system-strength-requirements/system-strength-requirements-methodology.pdf

[16] ——, "Power system requirements reference paper," 2020. [Online]. Available: Power-system-requirements.pdf(aemo.com.au)

[17] C. KARAWITA and U. ANNAKKAGE, *TB 909: Guidelines for Subsynchronous Oscillation Studies in Power Electronics Dominated Power Systems,JWG C4/B4.52*. CIGRE, 2023.

[18] K. Elkington, A. Isaacs, M. Davies, C. Smith, R. Gagnon, P. Christensen, and V. Lo, *TB 671: Connection of wind farms To Weak Ac Networks, WG B4.62*, 2016, no. December.

[19] L. Huang, H. Xin, Z. Li, P. Ju, H. Yuan, and G. Wang, "Identification of generalized short-circuit ratio for on-line stability monitoring of wind farms," *IEEE Transactions on Power Systems*, vol. 35, no. 4, pp. 3282–3285, 2020.

[20] M. O. Qays, I. Ahmad, D. Habibi, A. Aziz, and T. Mahmoud, "System strength shortfall challenges for renewable energy-based power systems: A review," *Renewable and Sustainable Energy Reviews*, vol. 183, p. 113447, 2023. [Online]. Available: https://www.sciencedirect.com/science/article/pii/S1364032123003040

[21] TERNA, "Benefici di sistema e analisi robustezza rete," *Terna*, 2023. [Online]. Available: https://download.terna.it/terna/Terna_Piano_Sviluppo_2023_Benefici_Sistema_analisi_Robustezza_Rete_8db2549a9e719c7.pdf

[22] Y. Zhu, T. C. Green, X. Zhou, Y. Li, D. Kong, and Y. Gu, "Impedance margin ratio: a new metric for small-signal system strength," 2023. [Online]. Available: https://www.techrxiv.org/users/693819/articles/683279-impedance-margin-ratio-a-new-metric-for-small-signal-system-strength

[23] C. Henderson, A. Egea-Alvarez, T. Kneuppel, G. Yang, and L. Xu, "Grid strength impedance metric: An alternative to scr for evaluating system strength in converter dominated systems," *IEEE Transactions on Power Delivery*, 2024.

[24] Q. Piraud, S. Dennetiere, and Y. Vernay, "Harmonic stability study for wind farm connection," *B4 International SC Meeting and Colloquium*, 2023.

[25] A. Jalali, B. Badrzadeh, J.Lu, N.Modi, and M.Gordon, "System strength challenges and solutions developed for a remote area of australian power system with high penetration of inverter-based resources," *CIGRE Science & Engineering*, vol. 20, p. 27, 2021.

[26] NERC, "Odessa disturbance texas events: May 9, 2021 and june 26," *NERC and Texas RE Staff Report*, 2021. [Online]. Available: https://www.nerc.com/pa/rrm/ea/Documents/Odessa_Disturbance_Report.pdf

[27] ——, "2022 odessa disturbance texas event: June 4, 2022," *NERC and Texas RE Staff Report*, 2022. [Online]. Available: https://www.nerc.com/comm/RSTC_Reliability_Guidelines/NERC_2022_Odessa_Disturbance_Report%20(1).pdf

[28] RTE, "Documentation technique de référence," https://www.services-rte.com/files/live//sites/services-rte/files/documentsLibrary/31-01-2023_COMPLET_1548_fr, 2023.

[29] P. Panciatici, G. Bareux, and L. Wehenkel, "Operating in the fog: Security management under uncertainty," *IEEE Power and Energy Magazine*, vol. 10, no. 5, pp. 40–49, 2012.

[30] RTE, "Reliability report," 2022.

[31] AEMO, "Power system security guidelines," 2023. [Online]. Available: https://www.aemo.com.au/-/media/Files/Electricity/NEM/Security_and_Reliability/Power_System_Ops/Procedures/SO_OP_3715%20Power-System-Security-Guidelines.pdf

[32] ——, "Power system stability guidelines," 2022. [Online]. Available: https://aemo.com.au/-/media/files/electricity/nem/security_and_reliability/congestion-information/power-system-stability-guidelines.pdf?la=en

[33] RTE, "R#space," 2020. [Online]. Available: https://codra.net/wp-content/uploads/2020/08/energy-sucess-story_RTE.pdf

[34] A. Bahmanyar, D. Ernst, Y. Vanaubel, Q. Gemine, C. Pache, and P. Panciatici, "Extended equal area criterion revisited: A direct method for fast transient stability analysis," *Energies*, vol. 14, no. 21, 2021. [Online]. Available: https://www.mdpi.com/1996-1073/14/21/7259

[35] ENTSOE, "Network code on high voltage direct current connections," 2016. [Online]. Available: https://www.entsoe.eu/network_codes/hvdc/

[36] H. Saad, A. Schwob, and Y. Vernay, "Study of resonance issues between hvdc link and power system components using emt simulations," 2018.

[37] S. Dennetiere, H. Saad, Y. Vernay, P. Rault, C. Martin, and B. Clerc, "Supporting energy transition in transmission systems: An operator's experience using electromagnetic transient simulation," *IEEE Power and Energy Magazine*, 2019.

[38] "Wind energy generation systems - Part 27-2: Electrical simulation models - Model validation," IEC Standard 61400-27-2:2020.

[39] E.-M. Karmani, E. Mberou, Y. Vernay, F. Morretton, and M. Thibert, "New modeling requirements for inverter based resources and storage system connection on the french transmission grid," in *MatPost 2023 Conference*, 11 2023.

[40] C. Cardozo, A. Guironnet, J.-L. Marin, T. Prevost, and G. Torresan, "Compliance criteria to assess rms model accuracy for wind power plants based on iec 61400-27-2," in *22nd Wind & Solar Integration Workshop*, 09 2023.

[41] AEMO, "Power system model guidelines," 2018. [Online]. Available: https://aemo.com.au/-/media/Files/Electricity/NEM/Security_and_Reliability/System-Security-Market-Frameworks-Review/2018/Power_Systems_Model_Guidelines_PUBLISHED.pdf

[42] ——, "Power system model guidelines," 2023. [Online]. Available: https://aemo.com.au/-/media/files/electricity/nem/security_and_reliability/system-security-market-frameworks-review/2023/power_systems_model_guidelines_2023_published_.pdf

[43] A. Dissanayaka and A. Isaacs, "System strength assessment of the panhandle system pscad study," 2016. [Online]. Available: https://www.ercot.com/files/docs/2016/03/01/panhandle_system_strength_study_feb_23_2016__public_.pdf

[44] A. Dissanayaka, J. Wiebe, and A. Isaacs, "Panhandle and south texas stability and system strength assessment," 2018. [Online]. Available: https://www.ercot.com/files/docs/2018/04/19/Panhandle_and_South_Texas_Stability_and_System_Strength_Assessment_March....pdf

[45] M. Amin and M. Molinas, "Small-signal stability assessment of power electronics based power systems: A discussion of impedance- and eigenvalue-based methods," *IEEE Transactions on Industry Applications*, 2017.

[46] L. Orellana, L. Sainz, E. Prieto-Araujo, M. Cheah-Mané, H. Mehrjerdi, and O. Gomis-Bellmunt, "Study of black-box models and participation factors for the positive-mode damping stability criterion," 2023.

[47] "Sras guideline system restart ancillary services," 2021. [Online]. Available: https://aemo.com.au/-/media/files/electricity/nem/security_and_reliability/ancillary_services/sras/sras-guideline-2021.pdf?la=en

[48] "Fiche i4 : Reconstitution de reseau et contribution au maintien d'un reseau separe," 2023. [Online]. Available: https://www.services-rte.com/files/live//sites/services-rte/files/documentsLibrary/Article%208.24%20-%20Cahier%20des%20charges%20des%20capacit%C3%A9s%20constructives%20pour%20un%20syst%C3%A8me%20HVDC_fr

[49] J. Loncle, P. Hondaa, J. M. A. Enjuanes, G. D. Castejón, A. D. Ferrer, L. Benard, J. Santana, V. Lehmann, T. Westerweller, and M. Häusler, "Feedback on inelfe france-spain hvdc project," 2016. [Online]. Available: https://www.e-cigre.org/publications/detail/b4-124-2016-feedback-on-inelfe-france-spain-hvdc-project.html

[50] J. Dumas, V. Terrier, F. Bienvenu, S. Finet, and N. Grisey, "Dynamic sizing of required balancing capacities: the operational approach in france," in *2023 19th International Conference on the European Energy Market (EEM)*. IEEE, Jun. 2023. [Online]. Available: http://dx.doi.org/10.1109/EEM58374.2023.10161932

[51] FinGrid, "Inertia of the nordic power system." [Online]. Available: https://www.fingrid.fi/en/electricity-market-information/InertiaofNordicpowersystem/

[52] MIGRATE, "D2.3: Lessons learned from monitoring & forecasting kpis on impact of pe penetration," 2018. [Online]. Available: https://ec.europa.eu/research/participants/documents/downloadPublic?documentIds=080166e5bf1893ec&appId=PPGMS

[53] Australian Energy Market Committee, "Rule determination national electricity amendment (managing the rate of change of power system frequency) rule 2017," 2017. [Online]. Available: Availableat:https://www.aemc.gov.au/sites/default/files/content/ed599cb5-91b5-45db-b157-99c0914ef9c3/ERC0214-Final-Determination-19-September-2017-published-version.pdf

[54] AEMO, "Inertia requirements methodology," 2018. [Online]. Available: https://www.aemo.com.au/-/media/files/electricity/nem/security_and_reliability/system-security-market-frameworks-review/2018/inertia_requirements_methodology_published.pdf

[55] ——, ""2023 inertia report"," 2023. [Online]. Available: https://aemo.com.au/-/media/files/electricity/nem/security_and_reliability/system-strength-requirements/2023-system-strength-report.pdf?la=en

[56] ICS Investigation Expert Panel, "Continental europe synchronous area separation on 08 january 2021," 2021. [Online]. Available: https://eepublicdownloads.azureedge.net/clean-documents/SOC%20documents/SOC%20Reports/entso-e_CESysSep_Final_Report_210715.pdf

[57] ——, "Continental europe synchronous area separation on 24 july 2021," 2022. [Online]. Available: https://eepublicdownloads.azureedge.net/clean-documents/Publications/2022/entso-e_CESysSep_210724_02_Final_Report_220325.pdf

[58] ENTSOE, "Project inertia – phase ii: Updated frequency stability analysis in long term scenarios, relevant solutions and mitigation measures," 2022. [Online]. Available: https://eepublicdownloads.blob.core.windows.net/public-cdn-container/clean-documents/sdc-documents/231108_Project_Inertia_Phase_II_First_Report_FOR_PUBLICATION_clean.pdf

[59] J. Song, M. Cheah-Mane, E. Prieto-Araujo, and O. Gomis-Bellmunt, "Short-circuit analysis of grid-connected pv power plants considering inverter limits," *International Journal of Electrical Power & Energy Systems*, vol. 149, p. 109045, 2023. [Online]. Available: https://www.sciencedirect.com/science/article/pii/S0142061523001023

[60] D. M. Schmieg, "P2021 gutachten zur nemo viii, los 1 - stabilität (kurzfassung)," 2021. [Online]. Available: https://www.netzausbau.de/SharedDocs/Downloads/DE/Bedarfsermittlung/2035/NEP/NEP2035_NEMOVIII-1.pdf?__blob=publicationFile

[61] AEMO, "2023 system strength report," 2023. [Online]. Available: https://aemo.com.au/-/media/files/electricity/nem/security_and_reliability/system-strength-requirements/2023-system-strength-report.pdf?la=en

[62] ——, "System strength impact assessment guidelines," 2023. [Online]. Available: https://aemo.com.au/-/media/files/stakeholder_consultation/consultations/nem-consultations/2022/ssrmiag/final-report/system-strength-impact-assessment-guideline_v2.pdf

[63] M. Zubiaga, J. J. Valera, C. Cardozo, T. Prevost, G. Denis, and M. Paolone, "D3.3 analysis of the synchronisation capabilities of bess power converters,," *OSMOSE*, 2022.

[64] E. Martínez Carrasco, M. P. Comech Moreno, M. T. Villén Martínez, and S. Borroy Vicente, "Improved faulted phase selection algorithm for distance protection under high penetration of renewable energies," 2020.

[65] V. Pradhan, N. George, O. Naidu, Z. Gajic, and S. Zubic, "Distance protection of inverter based renewables power evacuating lines and downstream network: Issues and mitigation approach, 2022 ieee pes innovative smart grid technologies - asia (isgt asia)," 2022.

[66] J. Quispe and E. Orduña, "Transmission line protection challenges influenced by inverter-based resources: a review," *Prot Control Mod Power Syst*, 2022. [Online]. Available: https://doi.org/10.1186/s41601-022-00249-8

[67] N. G. ESO, "Frequently asked questions stability pathfinder - phase 1 17 december 2019," *TBA*, 2019. [Online]. Available: https://www.nationalgrideso.com/document/185281/download

[68] S.Sproul, N.Modi, S.Cherevatskiy, A.Jalali, and S.Zabihi, "System strength support using grid-forming energy storage to enable high penetrations of inverter-based resources to operate on weak networks," *CIGRE Paris 2022*, 2022.

[69] Y. Zhou, R.Zhang, D.Kathriarachchi, J. Dennis, and S. Goyal, "Grid forming inverter and its applications to support system strength–a case study," *IET Gener. Transm. Distrib.*, vol. 17, pp. 391–398, 2023.

[70] Y. Cheng, "Preliminary assessment of grid forming inverter-based energy storage resources (gfm-ibr-esr) in the ercot grid," 2023. [Online]. Available: https://www.ercot.com/files/docs/2023/08/11/GFM_ERCOT_IBRWG(08112023).pdf

[71] [Online]. Available: https://www.agistin.eu/

[72] B. Badrzadeh, C. Cardozo, M. Hishida, S. Shah, I. Huq, N. Modi, and A. Morton, "Grid-forming inverters: Project demonstrations and pilots," *IEEE Power and Energy Magazine*, 2024.

[73] T. Engelbrecht, A. Isaacs, S. Kynev, J. Matevosyan, B. Niemann, A. J. Owens, B. Singh, and A. Grondona, "Statcom technology evolution for tomorrow's grid: E-statcom, statcom with supercapacitor-based active power capability," *IEEE Power and Energy Magazine*, 2023.

[74] "Guidance notes for grid forming plant," 2023. [Online]. Available: https://www.nationalgrideso.com/document/289921/download

[75] AEMO, "Voluntary specification for grid-forming inverters: Core requirements test framework," 2024. [Online]. Available: https://aemo.com.au/-/media/files/initiatives/engineering-framework/2023/grid-forming-inverters-jan-2024.pdf?la=en

[76] V. F. Guideline, "Vde fnn guideline : Grid forming behaviour of hvdc systems and dc-connected ppms," 2020. [Online]. Available: https://shop.vde.com/en/fnn-guideline-hvdc-systems-2

[77] "Specifications for grid-forming inverter-based resources," 2022. [Online]. Available: https://www.energy.gov/sites/default/files/2023-09/Specs%20for%20GFM%20IBRs%20Version%201.pdf

[78] "White paper: Grid forming functional specifications for bps-connected battery energy storage systems," 2023. [Online]. Available: https://www.nerc.com/comm/RSTC_Reliability_Guidelines/White_Paper_GFM_Functional_Specification.pdf

[79] ENTSOE, "Expert group on connection requirements for offshore systems – phase ii (proposal for the nc hvdc amendment)," 2023. [Online]. Available: https://eepublicdownloads.blob.core.windows.net/public-cdn-container/clean-documents/Network%20codes%20documents/GC%20ESC/CROS/Final_Report_-_Phase_2_01.pdf

[80] InterOpera, "D2.2 grid-forming functional requirements for hvdc converter stations and dc-connected ppms in multi-terminal multi-vendor hvdc systems," 2024. [Online]. Available: https://interopera.eu/wp-content/uploads/Docs/deliverables/InterOPERA-D2.2-GFM-functional-requirements-v1.1-Submitted-PU.pdf

[81] AEMO, "Nem engineering framework priority actions," 2022. [Online]. Available: https://aemo.com.au/-/media/files/initiatives/engineering-framework/2022/nem-engineering-framework-priority-actions.pdf?la=en&hash=F5297316185EDBD4390CDE4AE64F48BB

[82] ——, "Application of advanced grid-scale inverters in the nem," 2021. [Online]. Available: https://aemo.com.au/-/media/files/initiatives/engineering-framework/2021/application-of-advanced-grid-scale-inverters-in-the-nem.pdf

[83] A. Cerretti and T. SChaup, "Cenelec tc8x wg03 contribute: Acer workshop on rate of change of frequency and grid forming capabilities," 2023.

[84] B. Bahrani, M. H. Ravanji, B. Kroposki, D. Ramasubramanian, X. Guillaud, T. Prevost, and N.-A. Cutululis, "Grid-forming inverter-based resource research landscape: Understanding the key assets for renewable-rich power systems," *IEEE Power and Energy Magazine*, 2024.

[85] "A unique window of opportunity capturing the reliability benefits of grid-forming batteries," 2023. [Online]. Available: https://www.esig.energy/wp-content/uploads/2023/03/ESIG-GFM-batteries-brief-2023.pdf

[86] N. Modi, M. V. Escudero, K. Aramaki, X. Zhou, and P. Partinen, "High inverter-based resource integration: The experience of five system operators," *IEEE Power and Energy Magazine*, 2024.

[87] M. Hishida, T. Redfern, X. Li, D. Hughes, D. Duckwitz, and A. Knobloch, "Addressing transmission system operability challenges using multi-function large scale grid-forming bess solutions," *Energy Storage Conference 2023 (ESC 2023)*, 2023.

[88] A. Abdalrahman, Y.-J. Hafner, M. Kumar Sahu, and K. Kumar Nayak, "Grid Forming Control for HVDC Systems: Opportunities and Challenges," in *2022 24th European Conference on Power Electronics and Applications (EPE'22 ECCE Europe)*. Hanover, Germany: IEEE, Sep. 2022, pp. 1–10.

[89] C. Barker, "Voltage Source Converter (VSC) HVDC responses to disturbances and faults in AC systems which have low synchronous generation," CIGRE, Vienna, Austria, Tech. Rep., Sep. 2023.

[90] Y. Jiang Hafner and M. Manchen, "Stability Enhancement and Blackout Prevention by VSC Based HVDC," Bologna, Italy, 2011, p. 9.

[91] E. Rokrok, T. Qoria, A. Bruyere, B. Francois, and X. Guillaud, "Integration of a storage device to the DC bus of a grid-forming controlled HVDC interconnection," *Electric Power Systems Research*, vol. 212, p. 108601, Nov. 2022. [Online]. Available: https://linkinghub.elsevier.com/retrieve/pii/S0378779622006848

[92] X. Xiong, C. Wu, B. Hu, D. Pan, and F. Blaabjerg, "Transient Damping Method for Improving the Synchronization Stability of Virtual Synchronous Generators," *IEEE Trans. Power Electron.*, vol. 36, no. 7, pp. 7820–7831, Jul. 2021. [Online]. Available: https://ieeexplore.ieee.org/document/9303430/

[93] A. Narula, M. Bongiorno, M. Beza, J. R. Svensson, X. Guillaud, and L. Harnefors, "Impact of steady-state grid-frequency deviations on the performance of grid-forming converter control strategies," in *2020 22nd European Conference on Power Electronics and Applications (EPE'20 ECCE Europe)*. Lyon, France: IEEE, Sep. 2020, pp. P.1–P.10. [Online]. Available: https://ieeexplore.ieee.org/document/9215947/

[94] Q.-C. Zhong, P.-L. Nguyen, Z. Ma, and W. Sheng, "Self-Synchronized Synchronverters: Inverters Without a Dedicated Synchronization Unit," *IEEE Trans. Power Electron.*, vol. 29, no. 2, pp. 617–630, Feb. 2014. [Online]. Available: http://ieeexplore.ieee.org/document/6504534/

[95] Y. Mohamed and E. El-Saadany, "Adaptive Decentralized Droop Controller to Preserve Power Sharing Stability of Paralleled Inverters in Distributed Generation Microgrids," *IEEE Transactions on Power Electronics*, vol. 23, no. 6, pp. 2806–2816, Nov. 2008. [Online]. Available: http://ieeexplore.ieee.org/document/4696040/

[96] T. Qoria, "Grid-forming control to achieve a 100% power electronics interfaced power transmission systems," PhD Thesis, ENSAM, Lille, Nov. 2020.

[97] S. D'Arco, J. A. Suul, and O. B. Fosso, "Small-signal modelling and parametric sensitivity of a Virtual Synchronous Machine," in *2014 Power Systems Computation Conference*. Wrocław, Poland: IEEE, Aug. 2014, pp. 1–9. [Online]. Available: http://ieeexplore.ieee.org/document/7038410/

[98] O. Mo, S. D'Arco, and J. A. Suul, "Evaluation of Virtual Synchronous Machines With Dynamic or Quasi-Stationary Machine Models," *IEEE Trans. Ind. Electron.*, vol. 64, no. 7, pp. 5952–5962, Jul. 2017. [Online]. Available: http://ieeexplore.ieee.org/document/7781612/

[99] Qing-Chang Zhong, Phi-Long Nguyen, Zhenyu Ma, and Wanxing Sheng, "Self-Synchronized Synchronverters: Inverters Without a Dedicated Synchronization Unit," *IEEE Trans. Power Electron.*, vol. 29, no. 2, pp. 617–630, Feb. 2014. [Online]. Available: http://ieeexplore.ieee.org/document/6504534/

[100] M. Ashabani, F. D. Freijedo, S. Golestan, and J. M. Guerrero, "Inducverters: PLL-Less Converters With Auto-Synchronization and Emulated Inertia Capability," *IEEE Trans. Smart Grid*, vol. 7, no. 3, pp. 1660–1674, May 2016. [Online]. Available: http://ieeexplore.ieee.org/document/7258370/

[101] T. Qoria, E. Rokrok, A. Bruyere, B. Francois, and X. Guillaud, "A PLL-Free Grid-Forming Control With Decoupled Functionalities for High-Power Transmission System Applications," *IEEE Access*, vol. 8, pp. 197 363–197 378, 2020. [Online]. Available: https://ieeexplore.ieee.org/document/9240975/

[102] C. Arghir and F. Dorfler, "The Electronic Realization of Synchronous Machines: Model Matching, Angle Tracking, and Energy Shaping Techniques," *IEEE Transactions on Power Electronics*, vol. 35, no. 4, pp. 4398–4410, Apr. 2020. [Online]. Available: https://ieeexplore.ieee.org/document/8825565/

[103] B. B. Johnson, S. V. Dhople, A. O. Hamadeh, and P. T. Krein, "Synchronization of Parallel Single-Phase Inverters With Virtual Oscillator Control," *IEEE Transactions on Power Electronics*, vol. 29, no. 11, pp. 6124–6138, Nov. 2014. [Online]. Available: http://ieeexplore.ieee.org/document/6692879/

[104] S. D'Arco and J. A. Suul, "Phase Angle Feed-Forward Control for Improving the Power Reference Tracking of Virtual Synchronous Machines," *IEEE Transactions on Industry Applications*, pp. 1–13, 2023. [Online]. Available: https://ieeexplore.ieee.org/document/10286151/

[105] S. D'Arco, J. A. Suul, and O. B. Fosso, "Automatic Tuning of Cascaded Controllers for Power Converters Using Eigenvalue Parametric Sensitivities," *IEEE Trans. on Ind. Applicat.*, vol. 51, no. 2, pp. 1743–1753, Mar. 2015. [Online]. Available: https://ieeexplore.ieee.org/document/6891273

[106] J. Wang, L. Chen, Z. Liu, Z. Zhang, and X. Zhang, "Optimized Parameter Design of the Dual-Loop Control for Grid-Forming VSCs With *LC* Filters," *IEEE Transactions on Industry Applications*, vol. 58, no. 1, pp. 820–829, Jan. 2022. [Online]. Available: https://ieeexplore.ieee.org/document/9580573/

[107] J.-M. De Paris, H. Pinheiro, F. D. M. Carnielutti, V. F. Montagner, and D. M. Lima, "MPC for Grid Forming Converters with Current Limiting," in *IECON 2022 – 48th Annual Conference of the IEEE Industrial Electronics Society*. Brussels, Belgium: IEEE, Oct. 2022, pp. 1–5. [Online]. Available: https://ieeexplore.ieee.org/document/9968998/

[108] H. Wu and X. Wang, "Passivity-Based Dual-Loop Vector Voltage and Current Control for Grid-Forming VSCs," *IEEE Transactions on Power Electronics*, vol. 36, no. 8, pp. 8647–8652, Aug. 2021. [Online]. Available: https://ieeexplore.ieee.org/document/9311428/

[109] M. Nurunnabi, S. Li, and H. S. Das, "Control and Operation Evaluation of Grid-Forming Inverters with L, LC, and LCL Filters," in *2023 IEEE Power & Energy Society General Meeting (PESGM)*. Orlando, FL, USA: IEEE, Jul. 2023, pp. 1–5. [Online]. Available: https://ieeexplore.ieee.org/document/10253060/

[110] R. Rosso, X. Wang, M. Liserre, X. Lu, and S. Engelken, "Grid-Forming Converters: Control Approaches, Grid-Synchronization, and Future Trends—A Review," *IEEE Open J. Ind. Applicat.*, vol. 2, pp. 93–109, 2021. [Online]. Available: https://ieeexplore.ieee.org/document/9408354/

[111] G. Song, B. Cao, and L. Chang, "Review of Grid-forming Inverters in Support of Power System Operation," *Chinese Journal of Electrical Engineering*, vol. 8, no. 1, pp. 1–15, Mar. 2022. [Online]. Available: https://ieeexplore.ieee.org/document/9751441/

[112] D. B. Rathnayake, M. Akrami, C. Phurailatpam, S. P. Me, S. Hadavi, G. Jayasinghe, S. Zabihi, and B. Bahrani, "Grid Forming Inverter Modeling, Control, and Applications," *IEEE Access*, vol. 9, pp. 114 781–114 807, 2021. [Online]. Available: https://ieeexplore.ieee.org/document/9513281/

[113] E. Rokrok, T. Qoria, A. Bruyere, B. Francois, and X. Guillaud, "Effect of Using PLL-Based Grid-Forming Control on Active Power Dynamics Under Various SCR," in *IECON 2019 - 45th Annual Conference of the IEEE Industrial Electronics Society*. Lisbon, Portugal: IEEE, Oct. 2019, pp. 4799–4804. [Online]. Available: https://ieeexplore.ieee.org/document/8927648/

[114] L. Zhang, L. Harnefors, and H.-P. Nee, "Power-Synchronization Control of Grid-Connected Voltage-Source Converters," *IEEE Transactions on Power Systems*, vol. 25, no. 2, pp. 809–820, May 2010. [Online]. Available: http://ieeexplore.ieee.org/document/5308285/

[115] P. Imgart, A. Narula, M. Bongiorno, M. Beza, and J. R. Svensson, "A Cascaded Power Controller for Robust Frequency Ride-Through of Grid-Forming Converters," in *2022 IEEE Energy Conversion Congress and Exposition (ECCE)*. Detroit, MI, USA: IEEE, Oct. 2022, pp. 1–8. [Online]. Available: https://ieeexplore.ieee.org/document/9947721/

[116] P. Imgart, M. Bongiorno, J. R. Svensson, and M. Beza, "Stability Limits and Improved Robustness of Grid-Forming Converters With External Inertia-Emulation Loop," in *2023 25th European Conference on Power Electronics and Applications (EPE'23 ECCE Europe)*. Aalborg, Denmark: IEEE, Sep. 2023, pp. 1–8. [Online]. Available: https://ieeexplore.ieee.org/document/10264526/

[117] "Github L2EP EPMLAB, link to simulation files," Tech. Rep. [Online]. Available: https://github.com/l2ep-epmlab/VSC_Lib/tree/master/R2021a/Examples/PSCC

[118] T. Qoria, F. Gruson, F. Colas, X. Kestelyn, and X. Guillaud, "Current limiting algorithms and transient stability analysis of grid-forming VSCs," *Electric Power Systems Research*, vol. 189, p. 106726, Dec. 2020. [Online]. Available: https://linkinghub.elsevier.com/retrieve/pii/S0378779620305290

[119] B. Fan, T. Liu, F. Zhao, H. Wu, and X. Wang, "A Review of Current-Limiting Control of Grid-Forming Inverters Under Symmetrical Disturbances," *IEEE Open J. Power Electron.*, vol. 3, pp. 955–969, 2022. [Online]. Available: https://ieeexplore.ieee.org/document/9973369/

[120] A. D. Paquette and D. M. Divan, "Virtual Impedance Current Limiting for Inverters in Microgrids With Synchronous Generators," *IEEE Trans. on Ind. Applicat.*, vol. 51, no. 2, pp. 1630–1638, Mar. 2015. [Online]. Available: https://ieeexplore.ieee.org/document/6872529

[121] A. Narula, P. Imgart, M. Bongiorno, M. Beza, J. R. Svensson, and A. J.-P. Hasler, "Voltage-based Current Limitation Strategy to Preserve Grid-forming Properties Under Severe Grid Disturbances," *IEEE Open J. Power Electron.*, pp. 1–13, 2023. [Online]. Available: https://ieeexplore.ieee.org/document/10049117/

[122] T. Qoria, "Grid-forming control to achieve a 100% power electronics interfaced power transmission systems," Ph.D. dissertation, HESAM University, Ecole Nationale Supérieure d'Arts et Métiers, Nov. 2020.

[123] K. V. Kkuni and G. Yang, "Effects of current limit for grid forming converters on transient stability: analysis and solution," Jun. 2021, number: arXiv:2106.13555 arXiv:2106.13555 [cs, eess]. [Online]. Available: http://arxiv.org/abs/2106.13555

[124] K. G. Saffar, S. Driss, and F. B. Ajaei, "Impacts of Current Limiting on the Transient Stability of the Virtual Synchronous Generator," *IEEE Trans. Power Electron.*, vol. 38, no. 2, pp. 1509–1521, Feb. 2023. [Online]. Available: https://ieeexplore.ieee.org/document/9899737/

[125] L. Harnefors, M. Hinkkanen, U. Riaz, F. M. M. Rahman, and L. Zhang, "Robust Analytic Design of Power-Synchronization Control," *IEEE Trans. Ind. Electron.*, vol. 66, no. 8, pp. 5810–5819, Aug. 2019. [Online]. Available: https://ieeexplore.ieee.org/document/8490668/

[126] H. Wu and X. Wang, "Design-Oriented Transient Stability Analysis of PLL-Synchronized Voltage-Source Converters," *IEEE Trans. Power Electron.*, vol. 35, no. 4, pp. 3573–3589, Apr. 2020. [Online]. Available: https://ieeexplore.ieee.org/document/8820019/

[127] M. Chen, D. Zhou, and F. Blaabjerg, "Enhanced Transient Angle Stability Control of Grid-Forming Converter Based on Virtual Synchronous Generator," *IEEE Trans. Ind. Electron.*, vol. 69, no. 9, pp. 9133–9144, Sep. 2022. [Online]. Available: https://ieeexplore.ieee.org/document/9552499/

[128] Y. Laba, A. Bruyère, F. Colas, and X. Guillaud, "Virtual Power-Based Technique for Enhancing the Large Voltage Disturbance Stability of HV Grid-Forming Converters," in *2023 25th European Conference on Power Electronics and Applications (EPE'23 ECCE Europe)*. Aalborg, Denmark: IEEE, Sep. 2023, pp. 1–8. [Online]. Available: https://ieeexplore.ieee.org/document/10264486/

[129] ENTSO-E, "Stability Management in Power Electronics Dominated Systems: A Prerequisite to the Success of the Energy Transition," Jun. 2022.

[130] M. F. M. Arani and Y. A.-R. I. Mohamed, "Analysis and Performance Enhancement of Vector-Controlled VSC in HVDC Links Connected

to Very Weak Grids," *IEEE Transactions on Power Systems*, vol. 32, no. 1, pp. 684–693, Jan. 2017.
[131] J. F. Morris, K. H. Ahmed, and A. Egea-Àlvarez, "Analysis of Controller Bandwidth Interactions for Vector-Controlled VSC Connected to Very Weak AC Grids," *IEEE Journal of Emerging and Selected Topics in Power Electronics*, vol. 9, no. 6, pp. 7343–7354, Dec. 2021.
[132] X. Wang, M. G. Taul, H. Wu, Y. Liao, F. Blaabjerg, and L. Harnefors, "Grid-Synchronization Stability of Converter-Based Resources—An Overview," *IEEE Open Journal of Industry Applications*, vol. 1, pp. 115–134, 2020. [Online]. Available: https://ieeexplore.ieee.org/document/9181463/
[133] Y. Lamrani, L. Huang, F. Colas, X. Guillaud, F. Blaajberg, C. Cardozo, and T. Prevost, "Grid following converters stability study and control enhancements using an improved test setup," in *19th International Conference on AC and DC Power Transmission (ACDC 2023)*, vol. 2023, Mar. 2023, pp. 64–69.
[134] H. Yuan, H. Xin, D. Wu, Z. Li, X. Qin, Y. Zhou, and L. Huang, "Assessing Maximal Capacity of Grid-Following Converters With Grid Strength Constraints," *IEEE Transactions on Sustainable Energy*, vol. 13, no. 4, pp. 2119–2132, Oct. 2022. [Online]. Available: https://ieeexplore.ieee.org/document/9800140/
[135] Z. Zou, J. Tang, X. Wang, Z. Wang, W. Chen, G. Buticchi, and M. Liserre, "Modeling and Control of A Two-bus System With Grid-forming and Grid-following Converters," *IEEE Journal of Emerging and Selected Topics in Power Electronics*, pp. 1–1, 2022.
[136] S. Jiang and G. Konstantinou, "Generalized impedance model and interaction analysis for multiple grid-forming and grid-following converters," *Electric Power Systems Research*, vol. 214, p. 108912, Jan. 2023. [Online]. Available: https://linkinghub.elsevier.com/retrieve/pii/S0378779622009634
[137] H. Xin, Y. Wang, X. Liu, B. Tang, G. Yu, and L. Huang, "How Many Grid-Forming Converters do We Need? A Perspective From Power Grid Strength," Sep. 2022. [Online]. Available: http://arxiv.org/abs/2209.10465
[138] P. F. Mayer, M. Gordon, W.-C. Huang, and C. Hardt, "Improving grid strength in a wide-area transmission system with grid forming inverters," *IET Generation, Transmission & Distribution*, vol. n/a, no. n/a. [Online]. Available: https://onlinelibrary.wiley.com/doi/abs/10.1049/gtd2.12498
[139] Y. Lamrani, F. Colas, T. Van Cutsem, C. Cardozo, T. Prevost, and X. Guillaud, "On the Stabilizing Contribution of Different Grid-Forming Controls to Power Systems," Jan. 2024. [Online]. Available: https://www.techrxiv.org/users/688223/articles/680612-on-the-stabilizing-contribution-of-different-grid-forming-controls-to-power-systems?commit=98ac9b64fe0bab0ac532c8a1f090f8b5e39e3e0a
[140] ABB, "XLPE Submarine Cable Systems Attachment to XLPE Land Cable Systems - User's Guide Rev 5."
[141] RTE, "Article 8.3.3 – Trame de procédure de contrôle de conformité pour le raccordement d'une installation de production ou de stockage."
[142] ——, "Cahier des charges des Capacités Constructives Conditions générales - Unité de stockage non synchrone," Feb. 2021.
[143] E. Rokrok, T. Qoria, A. Bruyere, B. Francois, H. Zhang, M. Belhaouane, and X. Guillaud, "Impact of grid-forming control on the internal energy of a modular multilevel converter," in *2020 22nd European Conference on Power Electronics and Applications (EPE'20 ECCE Europe)*. Lyon, France: IEEE, Sep. 2020, pp. 1–10. [Online]. Available: https://ieeexplore.ieee.org/document/9215646/
[144] L. Zhao, Z. Jin, and X. Wang, "Analysis and Damping of Low-Frequency Oscillation for DC-Link Voltage-Synchronized VSCs," *IEEE Transactions on Power Electronics*, vol. 38, no. 7, pp. 8177–8189, Jul. 2023. [Online]. Available: https://ieeexplore.ieee.org/document/10089557/
[145] ——, "Small-Signal Synchronization Stability of Grid-Forming Converters With Regulated DC-Link Dynamics," *IEEE Transactions on Industrial Electronics*, vol. 70, no. 12, pp. 12 399–12 409, Dec. 2023. [Online]. Available: https://ieeexplore.ieee.org/document/10012586/
[146] N. Hatziargyriou, J. Milanovic, C. Rahmann, V. Ajjarapu, C. Canizares, I. Erlich, D. Hill, I. Hiskens, I. Kamwa, B. Pal, P. Pourbeik, J. Sanchez-Gasca, A. Stankovic, T. Van Cutsem, V. Vittal, and C. Vournas, "Definition and classification of power system stability – revisited & extended," *IEEE Transactions on Power Systems*, vol. 36, no. 4, pp. 3271–3281, 2021.